Structural behaviour of stainless steel frames subject to fire

MASTER THESIS

Author:
Guillermo Segura Valdivieso

Supervised by:
Enrique Mirambell Arrizabalaga

Master:
Ingeniería de Caminos, Canales y Puertos

Barcelona, June 2019

Department of Civil and Environmental Engineering

ABSTRACT

This master thesis investigates the thermal and mechanical response of stainless steel frames subjected to fire. Stainless steel is known to have a better behaviour at elevated temperatures than carbon steel, combined with its aesthetical appeal, corrosion resistance and higher mechanical properties, stainless steel structures may become an attractive alternative to carbon steel structures. The objective of this research is to assess the response of stainless steel frames subjected to fire and identify key parameters that rule their response at elevated temperatures.

An exhaustive calibration of the FE models has been carried out as a part of an extensive study of transient thermo-mechanical coupled models, which are needed to assess the response of stainless steel frames subjected to fire. In this direction, a simplified method to assess the influence of the cavity heat transfer on hollow section structures subjected to fire is presented.

Moreover, a comprehensive analysis of stainless steel frames subjected to fire is carried out, varying the boundary conditions, the material and the degree of utilization (load applied). Lastly, some conclusions about the current treatment of stainless steel structures under fire situation in European design codes are pointed out. Furthermore, the benefits that stainless steel structures provide in front of fire are verified in the three domains of fire resistance: load resistance, critical temperature and time resistance, being superior in all three domains to carbon steel structures. At the end of the present document, possible future works are highlighted.

RESUMEN

Esta tesis de master analiza la respuesta térmica y estructural de los pórticos de acero inoxidable sometidos a fuego. Es conocido que el acero inoxidable tiene un mejor comportamiento a temperaturas elevadas que el acero al carbono que, combinado con su atractivo estético, resistencia a la corrosión y mejores propiedades mecánicas, hace que las estructuras de acero inoxidable pueden convertirse en una alternativa atractiva a las estructuras de acero al carbono. El objetivo de esta investigación es evaluar la respuesta de los pórticos de acero inoxidable sometidos a fuego e identificar los parámetros clave que rigen su comportamiento a temperaturas elevadas.

Se ha llevado a cabo una calibración exhaustiva de modelos basados en elementos finitos como parte de un extenso estudio de modelos transitorios termo-mecánicos acoplados, los cuales son necesarios para evaluar la respuesta de los pórticos de acero inoxidable sometidos a fuego. En esta dirección, se presenta un método simplificado para evaluar la influencia de la transferencia de calor en la cavidad en estructuras de sección hueca sometidas a la acción del fuego.

Además, se lleva a cabo un análisis exhaustivo de los pórticos de acero inoxidable sometidos a fuego, variando las condiciones de contorno, el material y el factor de utilización (carga aplicada). Por último, se destacan algunas conclusiones sobre el tratamiento actual de las estructuras de acero inoxidable en situación de incendio en los códigos de diseño europeos. Asimismo, las ventajas que ofrecen las estructuras de acero inoxidable frente a fuego se confirman en los tres dominios de resistencia al fuego — resistencia mecánica, temperatura crítica y tiempo de resistencia— siendo superiores en todos ellos a las estructuras de acero al carbono. Al final del documento, se destacan posibles trabajos futuros en este tema.

ACKNOWLEDGEMENT

I would like to express my gratitude to my supervisor, Enrique Mirambell, who has guided me throughout this master thesis. Thanks to him I have improved my knowledge on steel structures.

I would also like to thank the rest of the steel group, and in particular Esther Real, for all the help and support they have given me.

CONTENTS

ABSTRACT 2

RESUMEN 3

ACKNOWLEDGEMENT 4

1. INTRODUCTION 10

1.1 BACKGROUND 10

1.2 RESEARCH OBJECTIVES 12

GENERAL OBJECTIVES 12

SPECIFIC OBJECTIVES 12

1.3 THESIS OUTLINE 13

2. STATE OF ART 16

2.1 INTRODUCTION 16

2.2 STAINLESS STEEL MATERIAL 16

STRESS-STRAIN RELATIONSHIP AT ROOM TEMPERATURE $20°C$ 19

STRESS-STRAIN RELATIONSHIP AT ELEVATED TEMPERATURES 24

2.3 FIRE EFFECTS ON STAINLESS STEEL 25

FIRE AS A PHYSICAL PHENOMENON 26

THERMAL STEEL PROPERTIES 28

2.4 DESIGN OF STEEL STRUCTURES SUBJECTED TO FIRE 29

FIRE ACTION (ACCIDENTAL LOAD COMBINATION) 32

STRUCTURAL DESIGN UNDER FIRE 32

2.5 TESTING THE RESPONSE OF STEEL STRUCTURES SUBJECTED TO FIRE 36

ISOTHERMAL CONDITIONS 36

ANISOTHERMAL CONDITIONS 37

3. NUMERICAL MODEL. CALIBRATION 39

3.1 ABAQUS PROGRAM 39

Heat transfer problem 40
Mechanical problem 41
Thermo-mechanical coupled problem 43
3.2 Validation of the numerical model 44
Thermal expansion effect 44
Temperature development of a steel member subjected to fire 46
Nonlinear material response due to temperature increase 47
Isothermal numerical test reproduction. Lateral torsional buckling 49
Anisothermal laboratory test reproduction 52
3.3 Heat transfer model for hollow sections 53
Introduction to the simplified model 54
Modelling of cavity radiation in Abaqus 55
Calibration of the simplified cavity radiation model 57

4. STUDY OF THE RESPONSE OF STAINLESS STEEL FRAMES UNDER FIRE 61

4.1 Basis for the study 61
Stainless steel frame design 61
Initial geometric imperfection 64
Residual stresses 65
4.2 Austenitic stainless steel frame response under fire 65
Structural response at room temperature 65
Thermo-mechanical coupled analysis 67
Normative application 69
4.3 Material comparison: stainless steel vs. carbon steel 72
Frame response under fire situation 74
4.4 Influence of boundary conditions 77
Previous calculations 77
Frame response under fire situation 79
4.5 Influence of the degree of utilization 81

5. CONCLUSIONS AND FUTURE WORKS 85

5.1 Summary 85
5.2 Numerical model 86

5.3 STAINLESS STEEL FRAMES.....87

5.4 FUTURE WORKS 88

BIBLIOGRAPHY 92

CHAPTER 1

1. INTRODUCTION

1.1 BACKGROUND

Stainless steels are iron allows with a minimum content of chromium of 10.5% and usually at least 50% of iron. When exposed to corrosive ambient stainless steel is able to form a very thin self-repairing chromium oxide layer, preventing further corrosion. Combining this with its excellent mechanical properties and aesthetic appearance lead to an increment of popularity of stainless steel in new constructions.

Fire represents a catastrophic threat to human life. Therefore, it is necessary that buildings are designed and constructed in order to resist long enough time to evacuate the occupants and to prevent or delay the structure collapse. It is known that mechanical properties of carbon and stainless steel get its mechanical properties reduced at elevated temperatures, but stainless steel exhibit greater fire resistance than carbon steel. This prove that stainless steel may be an attractive alternative for many design scenarios compared to carbon steel.

Figure 1.1: The Chrysler Building, New York.

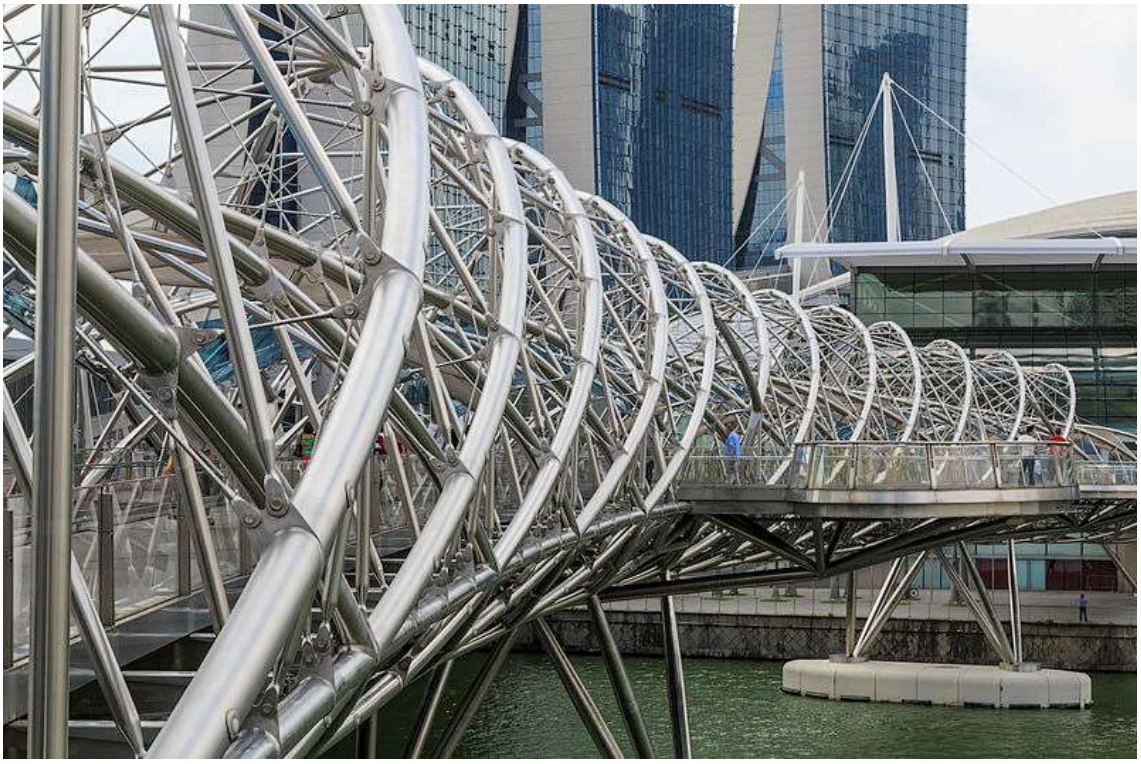

Figure 1.2: The Helix Bridge, Singapore.

1.2 RESEARCH OBJECTIVES

The main objectives of this research are to be able to model the behaviour of stainless steel frames subjected to fire and to understand the main parameters that rule their response. These objectives are subdivided in general and specific objectives.

General objectives

Optimal and efficient structure design is always a goal in construction. Although, higher stainless steel raw price makes it less competitive, economic-wise, compared to carbon steel. For this reason, an optimal stainless steel structure design has to benefit from the excellent corrosion resistance, aesthetic appearance, higher mechanical strength, fire resistance and sustainability that stainless steel has compared to carbon steel.

But, in order to reach an optimal design of stainless steel structures subjected to fire, extensive research on the behaviour of stainless steel frames under fire situation is required. With the objective to recognize key aspects to improve the fire design of stainless steel frames a parametric study needs to be performed.

Specific objectives

The specific objectives of this research are:

- Prove the validity of numerical models to reproduce the structural response of stainless steel frames subjected to fire. Determining the material parameters that rule the thermal and mechanical response of the structure.
- Assess the influence of the cavity heat transfer on the thermal and mechanical response of hollow cylinder section structures. If possible, develop of a simplified model to reproduce the effect of cavity radiation.
- Reproduce the effect of fire on stainless steel frames by means of numerical methods and more specifically solving the thermo-mechanical problem derived from the effect of the temperature increase on the mechanical response and the effect of the structure deflections of the thermal response. Moreover, compare the results obtained with the current European codes.

- Compare the response of stainless steel frames with carbon steel frame subjected to fire. Determine if stainless steel provides solid benefits in front of fire.
- Assess the influence of boundary condition on the response of stainless steel frames. Determining if fixed or pinned supports provides any benefits on the fire resistance of stainless steel frames.
- Clarify the influence of the degree of utilization on the fire resistance of stainless steel frames.

1.3 THESIS OUTLINE

This chapter includes a brief summary of stainless steel and the effects of fire on it. Then the general and specific goals of this research are defined and the outline of the document is presented.

Chapter 2 provides an overview of stainless steel chemical composition and its subdivision into 5 main groups: austenitic, ferritic, duplex, martensitic and precipitation hardening stainless steel. Then, the stress-strain relationship of stainless steel at room temperature and at elevated temperatures is introduced, followed by an introduction to fire as a physical phenomenon and how it is treated in the current European codes. Likewise, current design guidelines for stainless steel structures according to European codes are presented. The assessment of the response of stainless steel structures subjected to fire by means of experimental and numerical tests is also presented.

Chapter 3 is entirely dedicated to numerical methods. It is stated how the thermal and mechanical response can be modelled by means of numerical methods, followed by the validation of the numerical models used to reproduce the response of stainless steel frames under fire situation. Finally, the influence of the cavity radiation on the thermal and mechanical response of hollow cylinder section structures is determined and a simplified numerical model is presented to reproduce this effect.

In Chapter 4 the response of stainless steel frames is modelled by means of the numerical models already validated. Then, a parametric study of an austenitic stainless steel frame is carried out. Assessment of influence of the boundary conditions and the

degree of utilization is carried out and a comparative analysis of the response of stainless steel frames and carbon steel frames under fire situation is performed.

Finally, chapter 5 provides an overview of the results and the main conclusions obtained in this document and possible future areas of research.

CHAPTER 2

2. STATE OF ART

2.1 INTRODUCTION

This chapter provides an overview of the current knowledge needed to assess the response of stainless steel structures under fire. Firstly, the most important stress-strain models for stainless steel, including stress-strain models for elevated temperatures, are introduced. This is followed with an introduction to fire as a physical phenomenon, how the temperature of the gas develops over time and how fire is treated in the current structural design codes. Finally, a summary of the design guidelines for stainless steel structures under fire is presented.

2.2 STAINLESS STEEL MATERIAL

With the objective of reducing the life cycle cost in new buildings, stainless steel has seen its popularity increased due to its high structural strength, excellent corrosion resistance, aesthetic appearance and sustainability [1-3]. Furthermore, stainless steel structures performance under fire has been observed to be superior to carbon steel structures [4]. This makes stainless steel structures the best suitable solution for corrosive environments and where fire resistance may be decisive in the overall design.

Stainless steel is an alloy of iron, carbon, nickel and chromium in addition to molybdenum and manganese in few quantities. Stainless steel obtains its corrosion resistance from chromium, with a minimum content of 10.5% has a great affinity for oxygen, reacting with it and creating a protector layer and avoiding the reaction of iron with oxygen and preventing the corrosion.

The quantity of each metal in the alloy provides the stainless steel with different properties. The UNE EN 10088 [5] regulates the properties of the stainless steel depending on its chemical composition and sorting them in different grades. Stainless steel material can be divided into 5 groups [6]:

- **Austenitic stainless steel**: with a 17-18% of chromium and an 8-11% of nickel provides a high corrosion resistance, high ductility, are easily cold formed and are easy to weld. Its price is high compared to carbon steel due to the high content of nickel.
- **Ferritic stainless steel**: the most used ferritic stainless steels usually contain a percentage of chromium between 10.5% and 18%. They have nearly no nickel and show lower ductility than austenitic stainless steels, but maintain the corrosion resistance. Overall ferritic stainless steel is cheaper than austenitic stainless steel.
- **Duplex stainless steel**: also known as austenitic-ferritic stainless steels are a mix between austenitic and ferritic stainless steel. Usually contain a 20-26% of chromium, from 1% to 8% of nickel, less than a 5% of molybdenum and less than 0.3% of nitrogen.
- **Martensitic stainless steels**: have a high carbon content and can be strengthen by heat treatments. Usually used in hardened and tempered condition, which provides high strength and a moderate corrosion resistance. They are mainly used in cutlery, surgical instruments, industrial knives, wear plates and turbine blades.
- **Precipitation hardening stainless steels**: can be strengthen by heat treatments and are not usually welded. Their corrosion resistance is better than martensitic

stainless steel and similar to austenitic stainless steels. They are usually used in the aerospace industry.

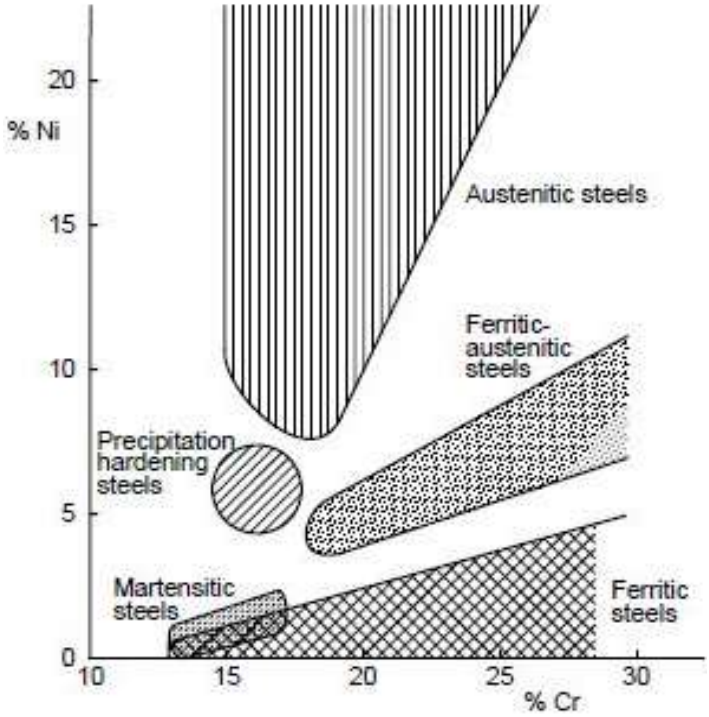

Figure 2.1: Different groups es of stainless steel depending on its nickel and chromium composition. [7]

The main drawback of stainless steel is its raw price which is quite higher than carbon steel, in addition, its price is very volatile because its tied to nickel market price, see Figure 2.2. But depending on the building typology, stainless steel higher resistance (reduced section thickness), better corrosion resistance (lower maintenance cost) and superior thermal properties (less isolation material) may make its overall price competitive in front of carbon steel.

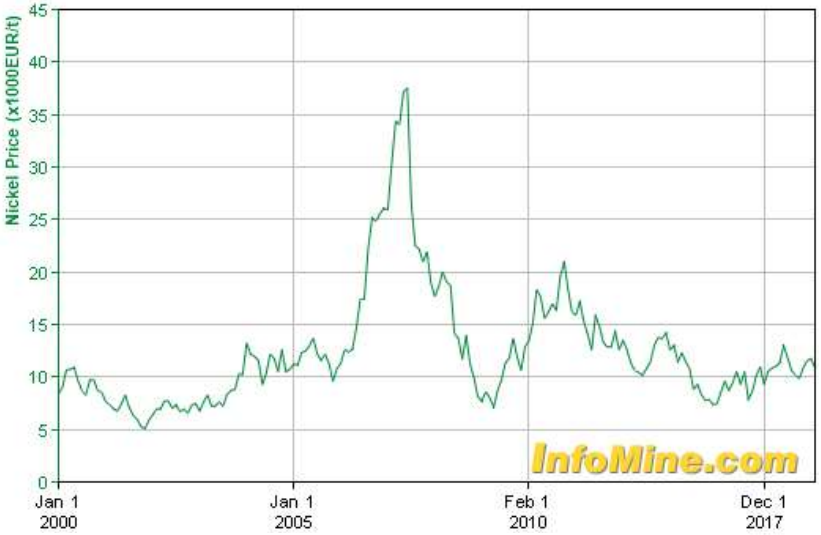

Figure 2.2: Nickel market price over time. (www.infomine.com)

Stress-strain relationship at room temperature $20℃$

Since the 20th century the stress-strain relationship of stainless steel has been widely studied [8]. A clearly nonlinear behaviour is described by this alloy, distinguished by its strength hardening. Initial models were based on carbon steel stress-strain relationship, following the Hooke's law up to a yield point and a perfect plastic behaviour after it. This first models were not able to model the nonlinearity of the stainless steel and no further progress was made until the Ramberg-Osgood model. Figure 2.3 shows the typical stress-strain relationship of carbon and stainless steel.

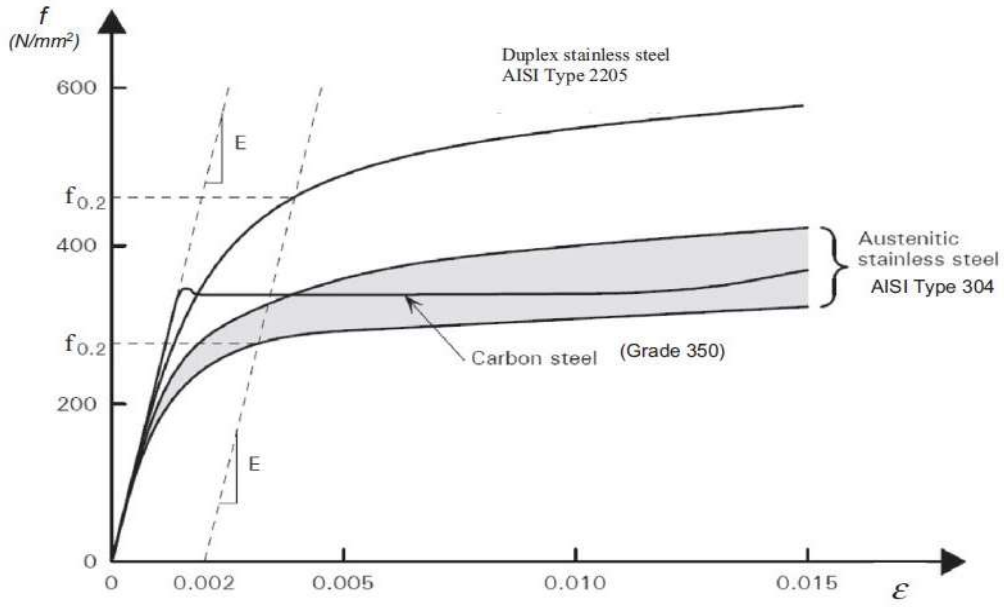

Figure 2.3: Typical stress-strain relationship of carbon and stainless steel [8].

Ramberg-Osgood (1943)

Ramberg-Osgood formulation [9], initially used for aluminium alloys, was found to be able to model the behaviour of steel alloys with a nonlinear stress-strain relationship, such as stainless steel.

$$\varepsilon = \frac{\sigma}{E_0} + K \cdot \left(\frac{\sigma}{E_0}\right)^n \tag{2.1}$$

The first term $\frac{\sigma}{E_0}$ is the elastic strain and the second term $K \cdot \left(\frac{\sigma}{E_0}\right)^n$ is the plastic strain, being K and n the parameters to be adjusted to represent the nonlinearity of the stress-strain relationship of the stainless steel, see Figure 2.4 and Figure 2.5.

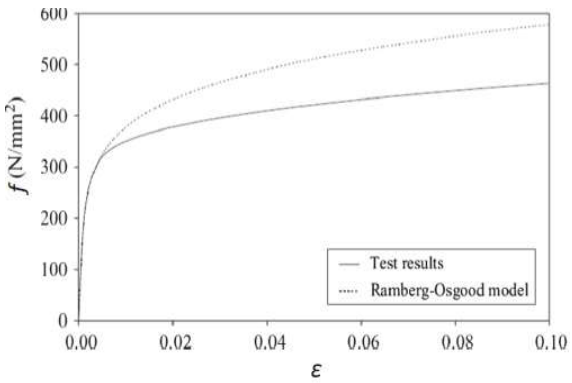

Figure 2.4: Initial approximation to the stainless steel stress-strain relationship by means of the original Ramberg-Osgood model [10].

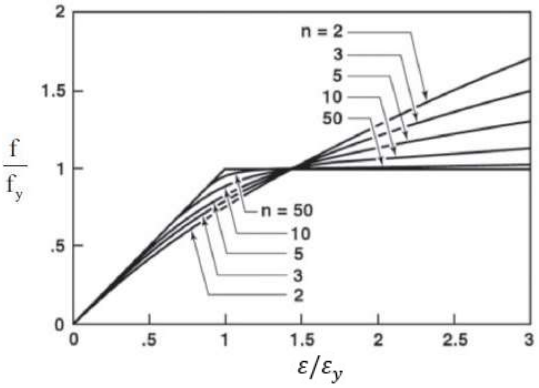

Figure 2.5: Influence of the parameter "n" to represent the nonlinearity of the stress-strain relationship [11].

Hill modification (1944)

Hill modified the Ramberg-Osgood model by determining the values of K and n [12]. Hill suggested to use as a yield stress the associated value to a plastic strain of 0.2%.

$$\varepsilon = \frac{\sigma}{E_0} + 0.002 \cdot \left(\frac{\sigma}{f_{0.2}}\right)^n$$
$$n = \frac{ln(20)}{ln\left(\frac{f_{0.2}}{f_{0.1}}\right)} \tag{2.2}$$

This model is included in the AS/NZS 4373:2001 [13] and the SEI/ASCE [14].

Mirambell-Real (2000)

After the study of the deflections of different hollow sections Mirambell and Real [15] proposed a two step model based on the Ramberg-Osgood formulation.

$$\varepsilon = \begin{cases} \frac{\sigma}{E_0} + 0.002 \cdot \left(\frac{\sigma}{f_{0.2}}\right)^n & for\ \sigma \le f_{0.2} \\ \frac{\sigma - f_{0.2}}{E_{0.2}} + \varepsilon^* \cdot \left(\frac{\sigma - f_{0.2}}{f_u - f_{0.2}}\right)^m + \varepsilon_{0.2} & for\ \sigma > f_{0.2} \end{cases} \tag{2.3}$$

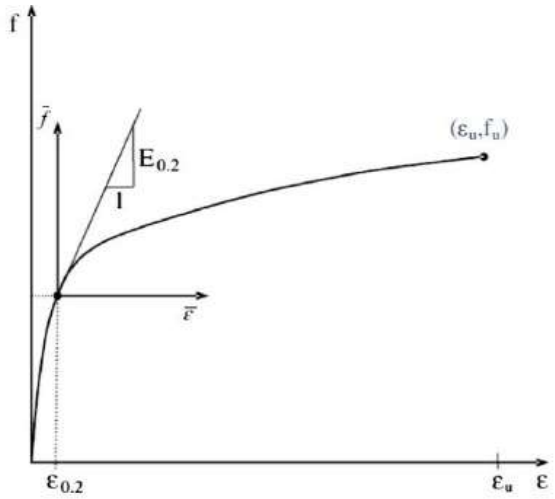

Figure 2.6: Representation of the two axis of reference used in the Mirambell-Real model. [15]

The first branch adopts the Ramberg-Osgood formulation up to the prof stress, and the second branch for higher stresses, adopts a new axis of reference, as is shown in Figure 2.6.

$$\varepsilon^* = \varepsilon_u - \varepsilon_{0.2} - \frac{f_u - f_{0.2}}{E_0} \tag{2.4}$$

$$\varepsilon_{0.2} = \frac{f_{0.2}}{E_0} + 0.002 \tag{2.5}$$

$$E_{0.2} = \frac{E_0}{1 + 0.002 \cdot n \cdot \left(\frac{E_0}{f_{0.2}}\right)} \tag{2.6}$$

ε^* is the ultimate plastic strain, $\varepsilon_{0.2}$ is the total strain at prof stress $\sigma_{0.2}$ and $E_{0.2}$ is the tangent Young modulus at prof stress. In total 6 parameters need to be calculated.

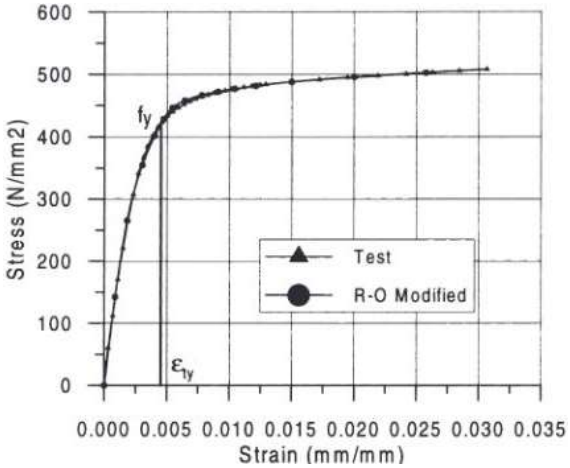

Figure 2.7: Comparation of the stress-strain relationship obtained with a laboratory test and the Mirambell-Real model [15].

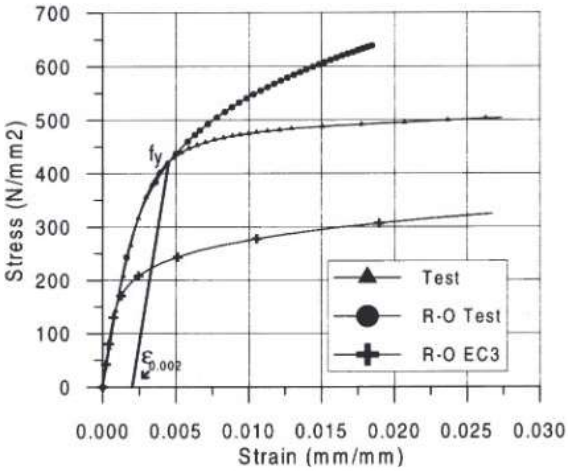

Figure 2.8: Comparation of the stress-strain relationship obtained with a laboratory test and the Ramberg-Osgood models in previous version of the EN 1993 [15].

As it can be seen in Figure 2.7 and Figure 2.8 the Mirambell-Real model shows a better agreement with the experimental test results than previous models.

Rassmussen modification (2003)

Rassmussen model [16] is exactly the same model as the developed by Mirambell and Real [15] but reduces the number of parameters to 3. This was achieved by assuming that the ultimate plastic strain ε^* is equal to the total ultimate strain ε_u with a minor error, which can be neglected. Reformulating the two step model (Eq. (2.3)) in terms of E_0, $f_{0.2}$ and m, the basic parameters of the original Ramberg-Osgood model are

$$\varepsilon = \begin{cases} \dfrac{\sigma}{E_0} + 0.002 \cdot \left(\dfrac{\sigma}{f_{0.2}}\right)^n & for\ \sigma \le f_{0.2} \\ \dfrac{\sigma - f_{0.2}}{E_{0.2}} + \varepsilon^* \cdot \left(\dfrac{\sigma - f_{0.2}}{f_u - f_{0.2}}\right)^m + \varepsilon_{0.2} & for\ \sigma > f_{0.2} \end{cases} \tag{2.7}$$

where

$$\varepsilon^* = 1 - \frac{f_{0.2}}{f_u} \tag{2.8}$$

$$\varepsilon_{0.2} = \frac{f_{0.2}}{E_0} + 0.002 \tag{2.9}$$

$$m = 1 + 3.5\left(\frac{f_{0.2}}{f_u}\right) \tag{2.10}$$

The nonlinearity of the stress-strain relationship is modelled by the parameter m which can be obtained by means of the ratio $f_{0.2}/f_u$, the value for that ratio was also provided by Rassmussen:

$$\frac{f_{0.2}}{f_u} = \begin{cases} 0.2 + 185 \cdot \dfrac{f_{0.2}}{E_0} & for\ austenitic\ and\ duplex \\ \dfrac{0.2 + 185 \cdot \dfrac{f_{0.2}}{E_0}}{1 - 0.0375 \cdot (n - 5)} & for\ other\ alloys \end{cases} \tag{2.11}$$

This model is included in the annex C of EN 1993-1-4 [17].

Gardner modification (2006)

Further studies done by Gardner et al [18] evidenced that the Mirambell-Real and Rassmussen models were only applicable to tensile behaviour, where necking appears (see Figure 2.9).

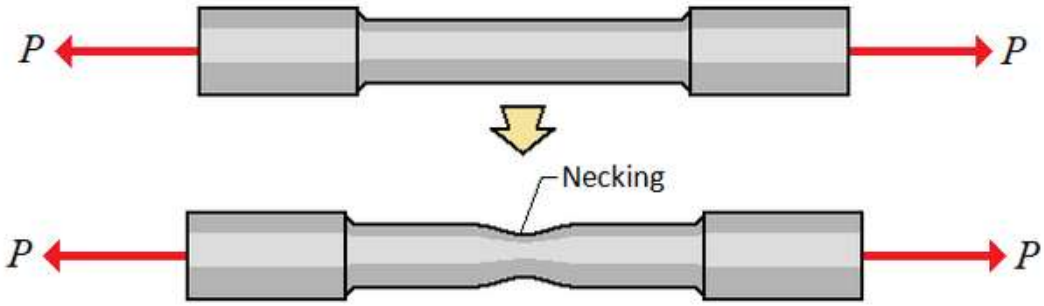

Figure 2.9: Necking effect in tensile test. (www.quora.com)

The new model used $f_{1.0}$ as a prof stress instead of f_u, because it was observed that calculated ultimate strains ε_u were much higher than the observed in real structures.

$$\varepsilon = \begin{cases} \dfrac{\sigma}{E_0} + 0.002 \cdot \left(\dfrac{\sigma}{f_{0.2}}\right)^n & for\ \sigma \le f_{0.2} \\ \dfrac{\sigma - f_{0.2}}{E_{0.2}} + \left[0.008 - (f_{1.0} - f_{0.2}) \cdot \left(\dfrac{1}{E_0} - \dfrac{1}{E_{0.2}}\right)\right] \cdot \left(\dfrac{\sigma - f_{0.2}}{f_{1.0} - f_{0.2}}\right)^m + \varepsilon_{0.2} & for\ \sigma > f_{0.2} \end{cases} \tag{2.12}$$

Figure 2.10 shows the stress-strain relationship of the same material using the diferent models presented.

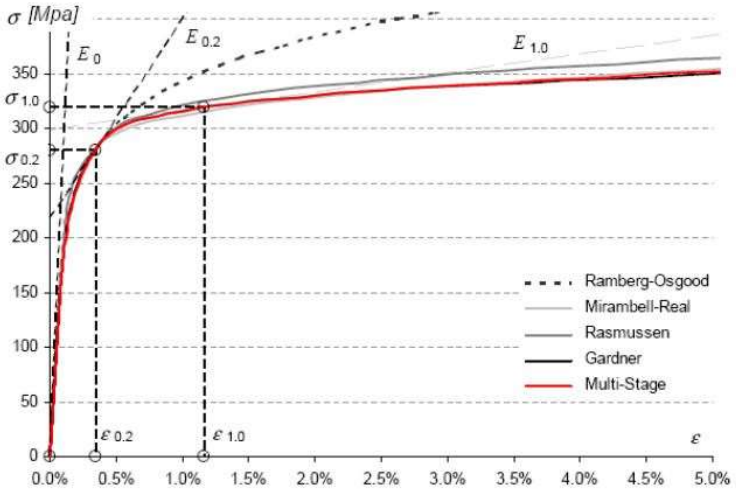

Figure 2.10: Comparation of the stress-strain relationship of a stainless steel obtained with the models presented [18].

Stress-strain relationship at elevated temperatures

Steel is known to lose its mechanical properties at elevated temperatures. For this reason, previous researchers [19, 20] showed that accurate representation of stress-strain relationship for stainless steel at elevated temperatures was fundamental to accurately assess the behaviour of stainless steel structures under fire.

The EN 1993-1-2, annex C [21] includes the current formulation of the stress-strain relationship at elevated temperatures for different grades of stainless steel. This formulation is based on previous studies of Abdella [22]. He proposed a stress-strain relationship for stainless steel alloys where the stress is presented by means of the strain; this was achieved by reversing the Ramberg-Osgood equations.

The formulation contained in EN 1993-1-2 [21] is very complex and with many parameters with no physical meaning, which is why researchers have proposed a new formulation (in revision) for the EN 1993-1-2 annex C [23] more consistent with the formulation for stainless steel at room temperature. Both stress-strain relationships are shown in Figure 2.11 and Figure 2.12.

Both formulations are based on the main parameters of a stainless steel ($E, f_{0.2}, f_2, f_u, \varepsilon_u$) at room temperature and use reduction factors ($k_E, k_{f_{0.2}}, k_{f_u}, k_{\varepsilon_u}$, …) at higher temperature to model the loss of resistances.

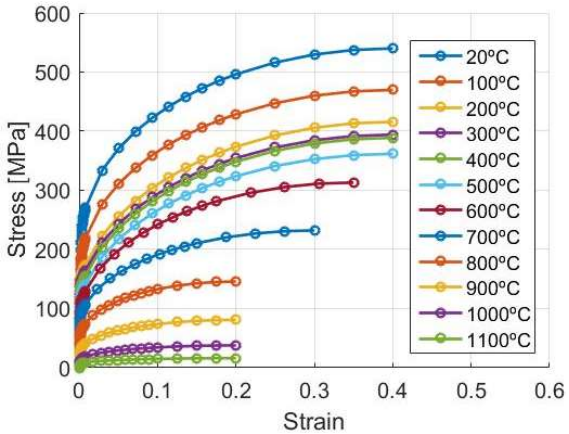

Figure 2.11: Stress-strain relationship of austenitic 1.4301 stainless steel according to the current EN 1993-1-2 [21].

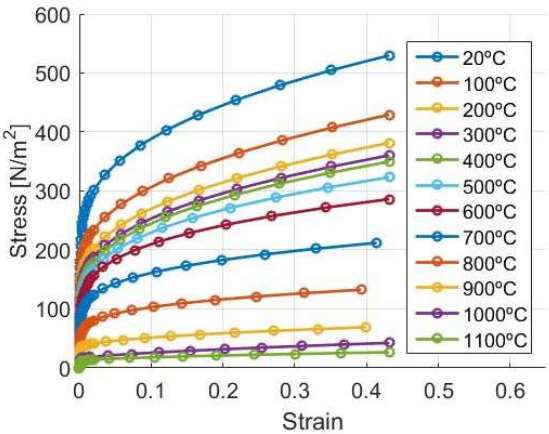

Figure 2.12: Stress-strain relationship of austenitic 1.4301 stainless steel according to the new proposal for the EN 1993-1-2, annex C [23].

Moreover, comparing the reduction factors of stainless steel and carbon steel it can be seen how carbon steel reduces its mechanical properties drastically from $500°C$ to $800°C$, whereas stainless steel exhibits higher reduction factors at elevated

temperatures, providing a first hint on stainless steel better behaviour under fire conditions.

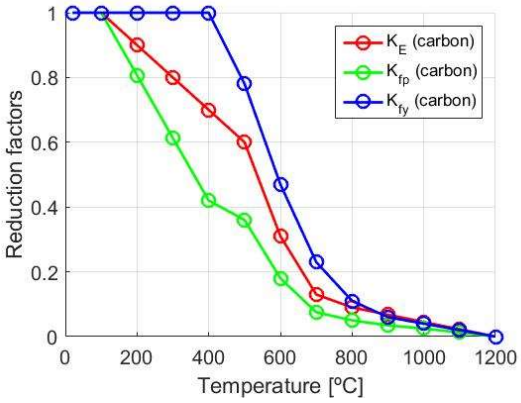

Figure 2.13: Reduction factors for carbon steel according to the EN 1993-1-2 [21].

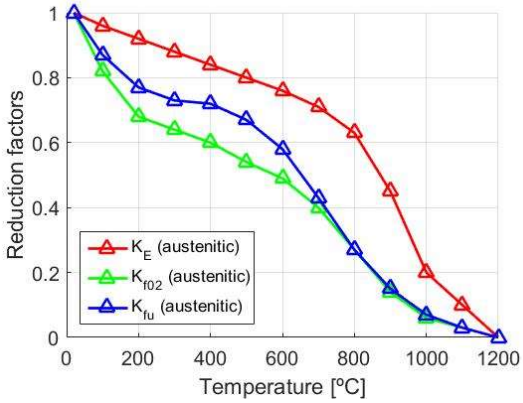

Figure 2.14: Reduction factors for austenitic (1.4301) steel according to the EN 1993-1-2, annex C [21].

2.3 FIRE EFFECTS ON STAINLESS STEEL

Fire is defined as the rapid oxidation of a material in the exothermic chemical reaction of combustion. This chemical process releases heat, light and it is an irreversible phenomenon. Combustion can only appear if the following conditions are present at the same time:

- **Heat:** Is necessary to provide a temperature high enough to reach the activation energy of the material in order to start the chemical reaction.
- **Fuel:** The material needed to have an exothermic reaction when oxidize.
- **Oxygen:** Plays the role of the comburent agent in the combustion reaction, providing oxygen to the material in order to oxidize it.
- **Chain reaction:** This phenomenon enables the continuity of the combustion reaction without the need of the initial heat source.

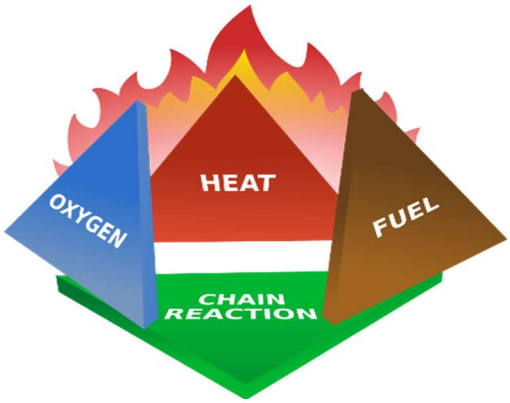

Figure 2.15: Representation of the 4 conditions needed in order to start fire.

Fire as a physical phenomenon

Fire development is divided into 4 stages [24]. These 4 stages are represented in Figure 2.16 and are the following:

- **Ignition:** Invisible particles to the human eye are released as temperature increases.
- **Growth:** Concentration of particles released increases becoming visible for human eye.
- **Fully developed:** If the concentration of oxygen is enough the concentration of particles create a flame. This phenomenon is known as flashover, it produces as a consequence a sudden increase in temperature and releasing toxic gases.
- **Decay (burnout):** As the material is consumed the fire development decays with time.

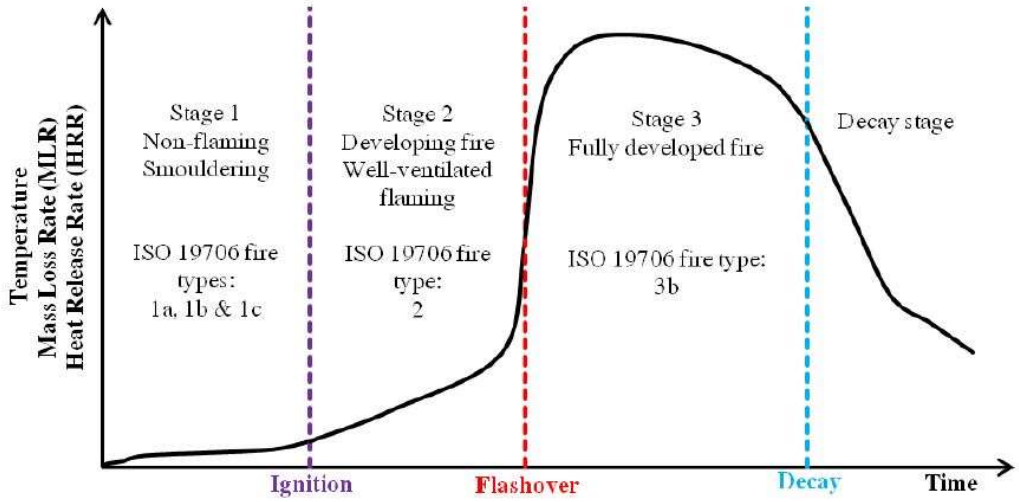

Figure 2.16: Temperature development over time of a real fire [25].

The gas temperature development over time varies depending on many factors, which may be different for each fire scenario. For this reason, in order to design structures subjected to fire normalized temperature-time curves are provided in EN 1993-1-2 [21].

The gas temperature increase generates a gradient of temperature in the gas itself and in the interface between the gas and the structure, this temperature gradient generates a heat flux from warmer zones to colder zones. This heat transfer can be explained by means of 3 physical phenomena [26]: radiation, convection and conduction.

Radiation heat transfer

Radiation is expelled by any body with a temperature higher than the absolute zero ($-273°C$). The amount of neat heat flux emitted by any body is determined by the Stephan-Boltzmann law (Eq. (2.13)):

$$\dot{h}_{net,r} = \phi \varepsilon_g \varepsilon_s \sigma [(\theta_g + 273)^4 - (\theta_s + 273)^4] \quad (2.13)$$

In this expression $\dot{h}_{net,r}$ is the net radiative heat flux (W/m^2) and ε_g and ε_s are the emissivities of the gas and the steel respectively, equal or smaller than one. This flux is ruled by the Stephan-Boltzmann constant $\sigma = 5.67 \cdot 10^{-8}\ W/m^2°K^{-4}$ and the configuration factor ϕ, which represents the fraction of radiation leaving the gas surface that is incident on the steel surface. The radiative heat flux is proportional to the fourth order temperature difference between the gas and the steel.

Convection heat transfer

Convection heat transfer appears due to air motion. This phenomenon produces a neat heat flux that is described by the Newton's law (Eq. (2.14)).

$$\dot{h}_{net,c} = \alpha_c \cdot (\theta_g - \theta_s) \quad (2.14)$$

Eq. (2.14) is ruled by the heat transfer convection coefficient α_c ($W/m^2°K$) and is proportional to the temperature difference between the gas and the steel element. Convection heat transfer is the main source of temperature increase at early fire stages, whereas radiation starts playing as a main role of heat transfer at high temperatures.

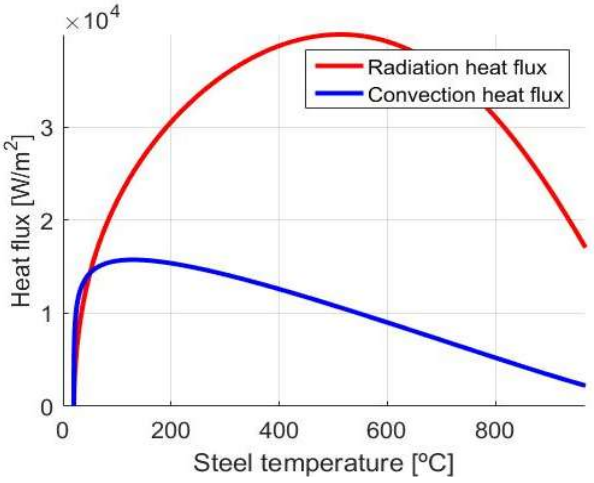

Figure 2.17: Comparation between radiation and convection heat flux in a stainless steel structure subjected to fire.

Fig 2.17 compares the radiation flux and the convection flux in a fictional circular stainless steel beam according to the formulation presented. The convection heat flux reaches a maximum when the gradient between the steel and the gas is maximum, whereas radiation heat flux reaches a peak at higher temperatures. Then, both decrease as the temperature gradient gets reduced.

Conduction heat transfer

Conduction heat flux appears due to a difference of temperature within an element from hotter parts to colder parts. Assuming an isotropic material, conductive heat flux depends on the thermal conductivity coefficient k ($\mathrm{W/m°K}$) and it is proportional to the gradient of the temperature (Eq. (2.15)).

$$q = -k\nabla\theta \tag{2.15}$$

The whole heat transfer problem can be described as a transient problem and is governed by Fourier's heat transfer equation (Eq. (2.16)) .

$$\rho_s c_s \frac{\partial\theta}{\partial t} - \nabla \cdot (k\nabla\theta) = \dot{q}_V \tag{2.16}$$

where ρ_s is the material density and c_s is the specific heat of the material, varying its value with the temperature. The volumetric heat source is represented by $\dot{q}_V$, in steel structures it has a null value.

Thermal steel properties

Stainless steel material properties can be found in EN1993-1-2, Annex C [21], where no differences between austenitic, ferritic and duplex thermal properties are stated. For stainless steel, the recommended values for the convection coefficient and emissivity are $\alpha_c = 25\mathrm{W/m^2°K}$ and $\varepsilon = 0.4$, respectively. It has been proposed by Gardner et al [27], different values for the convection coefficient ($\alpha_c = 35\mathrm{W/m^2°K}$) and emissivity ($\varepsilon = 0.2$) for stainless steel, where in some experiments reproduced more accurately the temperature of the steel member. For carbon steel, the recommended value for the emissivity is $\varepsilon = 0.7$. The convection coefficient for carbon steel is the same as in stainless steel $\alpha_c = 25\mathrm{W/m^2°K}$.

There are other properties that rule the whole heat transfer problem, these properties changing with temperature and are the following: specific heat, conductivity and thermal elongation. Thermal properties are inherent to the material, the EN1993-1-2, Annex C [21] only provides different formulations for carbon and stainless steel, but does not differentiate between the different types of stainless steel (austenitic, ferritic and duplex). Figure 2.18 and Figure 2.19 show the thermal properties of carbon and stainless steel using the formulation in EN 1993-1-2 [21], respectively.

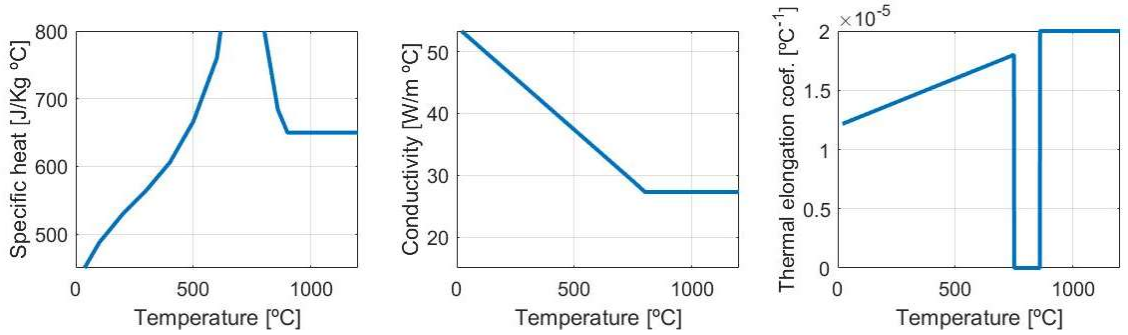

Figure 2.18: Specific heat, conductivity and thermal elongation coefficient of carbon steel at different temperatures according to EN 1993-1-2 [21].

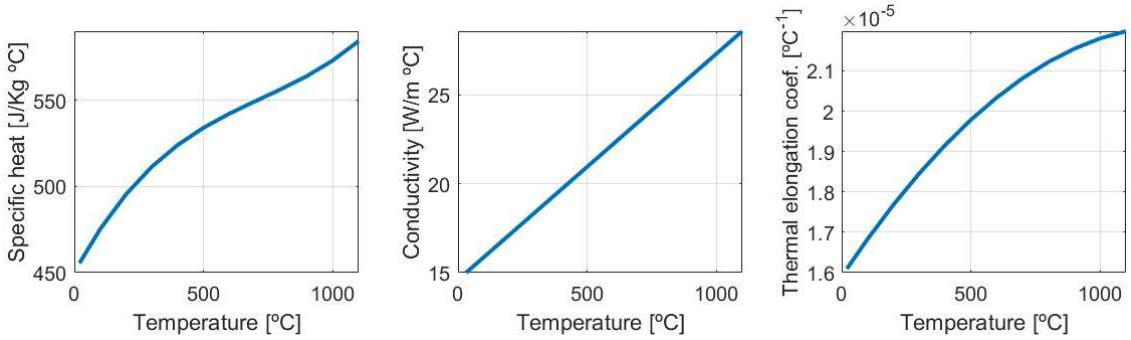

Figure 2.19: Specific heat, conductivity and thermal elongation coefficient of stainless steel at different temperatures according to EN 1993-1-2 [21].

The *Design Manual for Structural Stainless Steel* [6] and the new proposal for the EN1993-1-2, Annex C [23] provide different formulation for thermal properties, one for austenitic and duplex stainless steel and another for ferritic stainless steel.

2.4 DESIGN OF STEEL STRUCTURES SUBJECTED TO FIRE

Fire is a complex mix of physical phenomena meaning that only sophisticated methods, such as those based on computational fluid dynamics, can accurately reproduce the temperatures associated to a fire scenario [28, 29]. But this complex method is not of practical use when assessing the mechanical response of a steel structure. For this

reason, multiple normalized curves are proposed in European codes depending on the fire characteristics. Normalized curves assume a uniform temperature for all the gas volume.

For isolated compartments, when all the combustible material is ignited, after flashover point, it can be reasonably assumed a uniform gas temperature within the compartment [29]. Thus, the normalized curve ISO 834 (Eq. (2.17)) was included in the EN 1991-1-2 [30]

$$\theta_g = 20 + 345 \cdot log(8t + 1) \tag{2.17}$$

where θ_g is the gas temperature in ℃ in the compartment and t is the time in minutes. The ISO curve has been proved to be very conservative compared to recorded data [29]. Moreover, the normalized curve starts after the flashover point and does not allow a decay in temperature as the combustible material is used up (see Figure 2.20 and Figure 2.21).

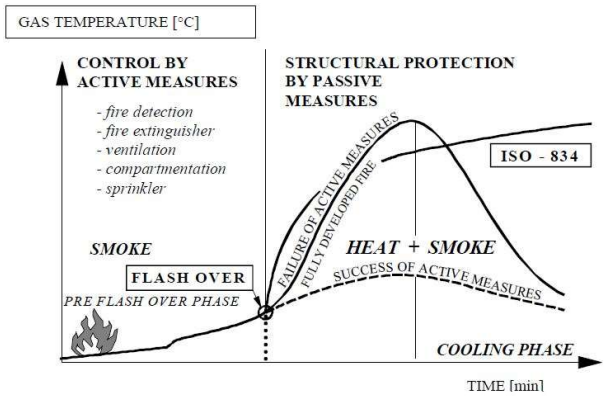

Figure 2.20: ISO 834 curve compared to a real fire with and without active measures [31].

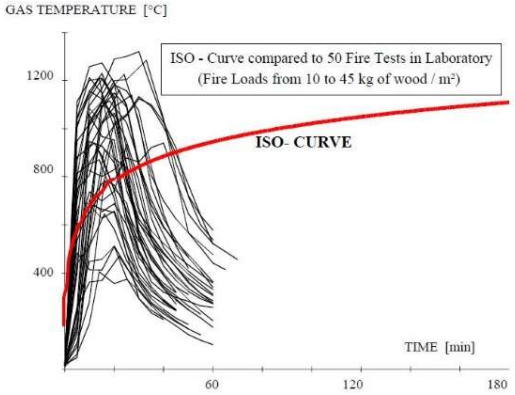

Figure 2.21: ISO 834 curve compared against 50 experimental laboratory tests [31].

Additionally, the EN 1991-1-2 [30] includes other standardized gas temperature curves for different types of fire situations: external fire (Eq. (2.18)) and hydrocarbon fire (Eq. (2.19)).

$$\theta_g = 660(1 - 0.687e^{-0.32t} - 0.313e^{-3.8t}) + 20 \tag{2.18}$$

$$\theta_g = 1080(1 - 0.325e^{-0.167t} - 0.675e^{-2.5t}) + 20 \tag{2.19}$$

For the external fire, θ_g is the gas temperature nearby the member. As it can be seen in Figure 2.22 the compartment fire (ISO 834) is the only curve that the gas temperature keeps growing continuously.

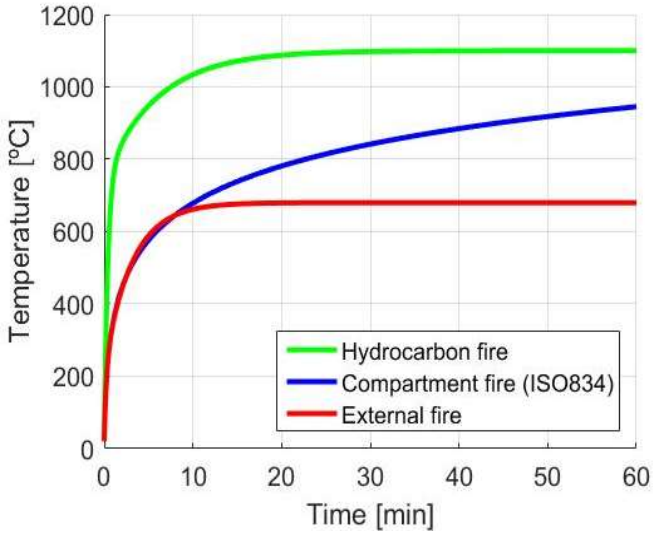

Figure 2.22: Different fire curves included in the EN 1993-1-2 [21].

Once the gas temperature is defined the heat transfer equations can be solved. Based on the equations presented (Eq. (2.13), Eq. (2.14), Eq. (2.15), Eq. (2.16)), the EN 1993-1-2 [21] incorporates a simplified formulation (Eq. (2.20)) to calculate the increase of temperature in a steel member assuming a uniform temperature within the cross-section.

$$\Delta\theta_{s,t} = k_{sh}\frac{A_m/V}{c_s\rho_s}\dot{h}_{net}\Delta t \tag{2.20}$$

The increase of temperature of the steel member $\Delta\theta_{s,t}$ is obtained at each time increment Δt (in minutes) and it depends on the section factor $S_m = A_m/V \geq 10m^{-1}$, the steel specific heat c_s, the steel density ρ_s and the correction factor k_{sh} that considers the shadow effect in non convex sections, such as I sections. The time increments must be always below to 5 seconds and the value of the net heat flux per unit of area $\dot{h}_{\mathrm{net}}$ is the sum of the net radiative heat flux and the net convective heat flux.

Fire action (accidental load combination)

According to the EN 1990 [32] the fire situation is considered as an accidental situation. Therefore, in Ultimate Limit State (ULS) the combination of actions in accidental situations is the following equation:

$$\sum_{j\geq 1}\gamma_{G,j}G_{k,j}+\gamma_A A_k+\gamma_{Q,1}\psi_{1,1}Q_{k,1}+\sum_{j\geq 1}\gamma_{Q,j}\psi_{2,j}Q_{k,j} \qquad (2.21)$$

where $G_{k,j}$ are the characteristic values of the permanent actions, A_k is the characteristic value of the accidental action, $Q_{k,1}$ is the characteristic value of the main variable action and $Q_{k,j}$ are the characteristic values of the rest of the variable actions. The values of the partial safety factor are $\gamma = 0$ for favourable actions and $\gamma = 1$ for unfavourable actions, the values of the simultaneity factor ψ can be obtained from the Spanish building code (CTE) [33].

	ψ_0	ψ_1	ψ_2
Sobrecarga superficial de uso (Categorías según DB-SE-AE)			
• Zonas residenciales (Categoría A)	0,7	0,5	0,3
• Zonas administrativas(Categoría B)	0,7	0,5	0,3
• Zonas destinadas al público (Categoría C)	0,7	0,7	0,6
• Zonas comerciales (Categoría D)	0,7	0,7	0,6
• Zonas de tráfico y de aparcamiento de vehículos ligeros con un peso total inferior a 30 kN (Categoría F)	0,7	0,7	0,6
• Cubiertas transitables (Categoría G)		(1)	
• Cubiertas accesibles únicamente para mantenimiento (Categoría H)	0	0	0
Nieve			
• para altitudes > 1000 m	0,7	0,5	0,2
• para altitudes ≤ 1000 m	0,5	0,2	0
Viento	0,6	0,5	0
Temperatura	0,6	0,5	0
Acciones variables del terreno	0,7	0,7	0,7

(1) En las cubiertas transitables, se adoptarán los valores correspondientes al uso desde el que se accede.

Figure 2.23: Values for the simultaneity factor, reproduction of table 4.2 of the CTE [33].

Structural design under fire

The objective of the structural design under fire conditions is to avoid the premature collapse of the structure. The goal of resisting enough time before the structure collapse is to guarantee the evacuation of the whole building. The Spanish building code (CTE) [33], includes different time resistance for each type of building to guarantee its

evacuation, as shown in Figure 2.24. The time resistance of a building is related to the importance and the use of the building.

Uso del *sector de incendio* considerado [1]	Plantas de sótano	Plantas sobre rasante *altura de evacuación* del edificio		
		<15 m	<28 m	≥28 m
Vivienda unifamiliar [2]	R 30	R 30	-	-
Residencial Vivienda, Residencial Público, Docente, Administrativo	R 120	R 60	R 90	R 120
Comercial, Pública Concurrencia, Hospitalario	R 120 [3]	R 90	R 120	R 180
Aparcamiento (edificio de uso exclusivo o situado sobre otro uso)		R 90		
Aparcamiento (situado bajo un uso distinto)		R 120 [4]		

Figure 2.24: Time resistances recommendations, reproduction of table 3.1 of CTE [33].

In order to avoid failure in fire situation, the load-bearing capacity ($R_{fi,d,t}$) of a steel member should be maintained under a combination of actions ($E_{fi,d}$) for a time t (Eq. (2.22)).

$$E_{fi,d} \leq R_{fi,d,t} \tag{2.22}$$

The time t should be at least the time resistance and it can be converted into a temperature using the simplified formulation included in EN 1993-1-2 [21] (Eq. (2.20)). The temperature at which the structure cannot resist the loads applied is known as the critical temperature θ_{cr}. Thus, the equation (Eq. (2.22)) can be rewrite in terms of temperatures

$$\theta_t \leq \theta_{cr} \tag{2.23}$$

where θ_t is the temperature of the member at a time t and θ_{cr} is the critical temperature at which the structure collapses. The critical temperature can be obtained by means of the simplified equation presented in the EN1993-1-2 [21], (Eq. (2.24)). This equation applies to structural elements not susceptible to buckling subjected to fire in their 4 faces.

$$\theta_{cr} = 39.19 \cdot ln\left(\frac{1}{0.9674 \cdot \mu_0^{3.833}} - 1\right) + 482 \tag{2.24}$$

Therefore, the design parameters for steel structures in fire design situation are the critical temperature of the element and the time resistance, which are directly related to the degree of utilization μ_0 (Eq. (2.25)), where $E_{fi,d}$ is the design effect of actions for

the fire design situation according to the EN 1991-1-2 [21] and $R_{fi,d,0}$ is the corresponding design resistance of the steel member at temperature 20℃

$$\mu_0 = \frac{E_{fi,d}}{R_{fi,d,0}} \tag{2.25}$$

There is no specific formulation for stainless steel at elevated temperatures in the EN 1993-1-2 [21] neither in the EN 1993-1-4 [17], but there have been multiple studies [34-37] proving that stainless steel structures under fire cannot be designed according to the carbon steel formulation. For this reason, specific formulation for structural stainless steel is included in the *Design Manual for Stainless Steel* [6] and in the new proposal for EN 1993-1-2 annex C [23].

Even thought, right now, the formulation to be used for stainless steel under fire is the carbon steel formulation included in the EN 1993-1-2 [21], using specific stainless steel parameters presented in EN 1993-1-4 [17], which is far away from the optimal design. The formulation to be applied depends on the section classification.

Non slender sections

Non slender sections (Class 1, Class 2 or Class 3 sections) are those that local buckling develops after reaching the yield stress f_y in the extreme compression fibre, for stainless steel f_y can be assumed to be $f_{0.2}$ according to EN 1993-1-4 [17].

Once the resistance time t needed is known and the temperature θ_t of the member at that time has been calculated, the verification of the Ultimate Limit State (Eq. (2.22)) must be done according to the formulation included in the EN 1993-1-2 [21], presented below.

For tensile members the design section resistance $N_{fi,\theta,Rd}$ at elevated temperature θ_t can be obtained according to Eq. (2.26)

$$N_{fi,\theta,Rd} = k_{y,\theta} N_{Rd} \left(\frac{\gamma_{M,0}}{\gamma_{M,fi}} \right) \tag{2.26}$$

where $k_{y,\theta}$ is the yield stress reduction factor ($k_{0.2,\theta}$ for stainless steel), N_{Rd} is the design tensile resistance at temperature 20℃ and $\gamma_{M,0}$ and $\gamma_{M,fi}$ are the partial factors at room temperature and under fire conditions respectively.

For compressed members, the design compression resistance of the section $N_{b,fi,\theta,Rd}$ is obtained by reducing the cross-section capacity by the parameter χ_{fi} in order to consider buckling effects.

$$N_{b,fi,\theta,Rd} = \chi_{fi} k_{y,\theta} A f_y \left(\frac{\gamma_{M,0}}{\gamma_{M,fi}}\right) \tag{2.27}$$

$$\chi_{fi} = \frac{1}{\phi_\theta + \sqrt{\phi_\theta^2 - \bar{\lambda}_\theta^2}} \tag{2.28}$$

$$\phi_\theta = 0.5\left(1 + \alpha\bar{\lambda}_\theta + \bar{\lambda}_\theta^2\right) \tag{2.29}$$

For beams laterally restrained the design bending resistance of the cross-section $M_{fi,\theta,Rd}$ at temperature θ_t is obtained as shown in Eq. (2.30)

$$M_{fi,\theta,Rd} = k_{y,\theta} M_{Rd} \left(\frac{\gamma_{M,0}}{\gamma_{M,fi}}\right) \tag{2.30}$$

where M_{Rd} is the design moment resistance at room temperature. Whereas, for laterally unrestrained beams the design bending resistance $M_{b,fi,\theta,Rd}$ can be obtained applying the reduction factor $\chi_{LT,fi}$ that considers the effect of lateral torsional buckling.

$$M_{b,fi,\theta,Rd} = \chi_{LT,fi} k_{y,\theta} W f_y \left(\frac{\gamma_{M,0}}{\gamma_{M,fi}}\right) \tag{2.31}$$

In this expression W is the section modulus (W_{pl} for Class 1 and Class 2 sections and W_{el} for Class 3 sections). The factor $\chi_{LT,fi}$ is obtained according to Eq. (2.32) and Eq. (2.33).

$$\chi_{LT,fi} = \frac{1}{\phi_{LT,\theta} + \sqrt{\phi_{LT,\theta}^2 - \bar{\lambda}_{LT,\theta}^2}} \tag{2.32}$$

$$\phi_{LT,\theta} = 0.5\left(1 + \alpha\bar{\lambda}_{LT,\theta} + \bar{\lambda}_{LT,\theta}^2\right) \tag{2.33}$$

The factors χ_{fi} and $\chi_{LT,fi}$ are obtained according to the carbon steel curves that in fire situations do to not have a horizontal platoon for low values of non-dimensional slenderness $\bar{\lambda}_\theta$ or $\bar{\lambda}_{LT,\theta}$. This has become a topic of discussion between researches, for instance, the *Design Manual for Structural Stainless Steel* [6] includes a horizontal platoon for stainless steel formulation under fire conditions, see Figure 2.25, increasing

its resistance at elevated temperatures compared to carbon steel, whereas the new proposal of the EN 1993-1-2, annex C [23] this platoon is not included.

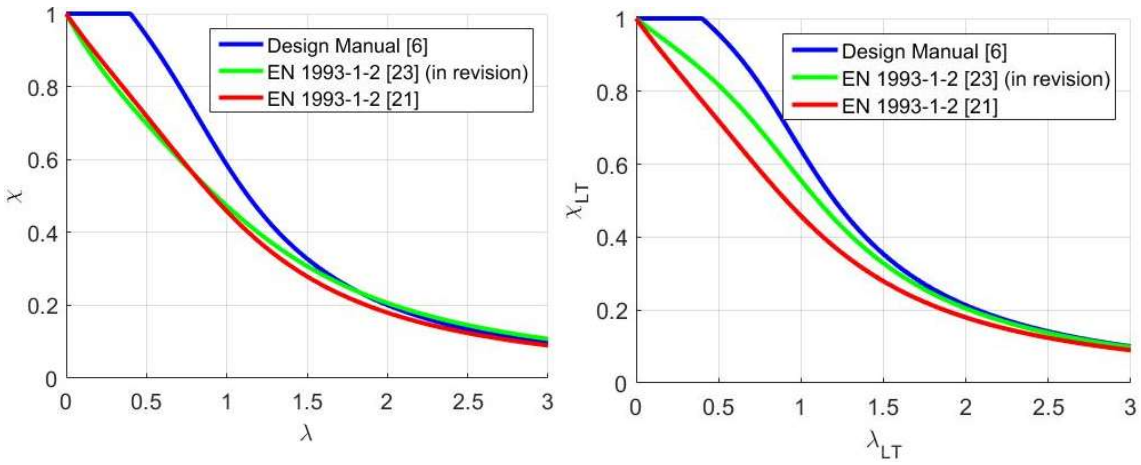

a) Flexural buckling *b) Lateral torsional buckling*

Figure 2.25: Comparation of the buckling curves for austenitic (1.4301) hollow section between the current EN 1993-1-2 [21], the Design Manual for Structural Stainless Steel [6] and the new proposal for the EN 1993-1-2, annex C [23] (in revision).

Slender sections

Slender sections (Class 4 sections) are those that develop local buckling before reaching in any of its fibres the elastic limit f_y. In this case, the cross-section verification (Eq. (2.22)) is considered to be fulfilled when $\theta_t \leq \theta_{cr}$ (Eq. (2.23)) is accomplished, using always $\theta_{cr} = 350℃$. Meaning that the temperature may never exceed $350℃$ in Class 4 sections.

This limitation has been a topic of discussion between researchers and, for instance, the *Design Manual for Stainless Steel* [6] and the proposal for the EN 1993-1-2, annex C [23] include specific formulation for Class 4 stainless steel sections.

2.5 TESTING THE RESPONSE OF STEEL STRUCTURES SUBJECTED TO FIRE

When assessing the structural response of steel structures at elevated temperatures by means of experimental or numerical tests, it can be done in two ways: under isothermal conditions or under anisothermal conditions.

Isothermal conditions

An isothermal test consists on increasing the temperature of the whole structure to a constant uniform temperature. Then, the applied load is gradually increased until

failure. Even thought, isothermal tests do not totally reproduce the reality of fire situations, because it ignores the effect of a nonuniform temperature distribution and obviate the effect of a non-uniform temperature increase on the structure. In any case, these isothermal tests are the most common tests done, mainly because they are easily reproduced with numerical models and isolates the structural response from the heat transfer problem.

For instance, most of the laboratory and numerical test used to obtain the χ- $\bar{\lambda}$ curves included in the EN 1993-1-2 [21] have been done under isothermal conditions.

Anisothermal conditions

Anisothermal test are carried out applying a constant load, usually this load is chosen as the equivalent of a degree of utilization μ_0, then the fire starts and increases the structure temperature until it fails.

As in real building fires, the structure is already loaded when the fire starts and it increases the temperature of the structure increases non uniformly until failure. Therefore, anisothermal tests reproduce more accurately the reality of a structure under fire. The main drawback of anisothermal tests is that are more difficult to numerically reproduce compared to isothermal tests.

CHAPTER 3

3. NUMERICAL MODEL. CALIBRATION

Cost of the required equipment to test steel structures subjected to fire and moreover the cost of this kind of experiments is elevated. For these reasons, being capable to model the behaviour of steel structures under fire using numerical methods have become a goal for most of the researchers on this field.

The assessment of the response of a steel structure under fire by means of numerical methods allows to not only reduce the cost of further investigations on this field, but also allows to do parametric studies of different structural types, materials and thermal and mechanical boundary conditions.

3.1 ABAQUS PROGRAM

Abaqus is a finite element analysis package known to be able to reproduce highly nonlinear problems, including heat transfer problems, nonlinear structural analysis and transient thermo-mechanical coupled problems [38]. The assessment of the response of a stainless steel structure under fire involves all these kinds of nonlinear problems. Furthermore, Abaqus is able to model structures using linear elements, shell elements and solid elements.

In real fire situations the heat transfer between the gas and the steel structure is affected by the deflections of the structure, likewise the response of the steel structure is directly affected by the temperature of it and therefore by the heat transfer problem, this is known as a transient thermo-mechanical coupled problem. Even thought, if fire is not modelled by advanced fluid dynamics models and is modelled with a simplified uniform gas temperature curve (ISO 834) the heat transfer problem may not be much affected by the structural response. As the gas temperature is only dependent on time, such temperature is included in numerical models as a boundary condition on the section surface. For this reason, many researchers model the response of a steel structure under fire solving first the heat transfer problem and then solving the nonlinear structural problem using the temperature field at each time step. This is known as a sequentially thermo-mechanical problem.

Heat transfer problem

Heat transfer problem is described by the differential equation (3.1). In order to be able to obtain the temperature field along the time by means of numerical method the weak form of the differential equation is obtained (see Eq. (3.2)). Then, the structure is discretised using finite elements, obtaining a system of equations that must be solved at each time increment in order to obtain the structure temperature.

$$\rho_s c_s \frac{\partial \theta}{\partial t} - \nabla \cdot (k \nabla \theta) = \dot{q}_V \tag{3.1}$$

$$\boldsymbol{K_\theta \theta} = \boldsymbol{f_\theta} \tag{3.2}$$

In this equation $\mathbf{K_\theta}$ is the so-called stiffness matrix of the thermal problem, $\boldsymbol{\theta}$ is the temperature vector and $\mathbf{f_\theta}$ is the source term. Since heat transfer problems are nonlinear and time dependent problems, the Newton-Raphson method is used as a root finding method to obtain the temperature of the whole structure at each time increment.

The radiation heat transfer and convection heat transfer are numerically modelled as two boundary conditions applied to the structure surfaces. These boundary conditions reproduce the heat transfer equations Eq. (2.13) and Eq. (2.14). For meshing purposes,

the structure geometry can be discretized in shell elements (DS4) that include the thermal degrees of freedom required to solve the heat transfer analysis.

Mechanical problem

Aside from the heat transfer problem, the purely mechanical problem of the structure is also solved. The Euler-Bernoulli equation for static beams (Eq. (3.3)) is transformed into its weak form and the structure is discretized in finite elements, obtaining a system of equations (Eq. (3.4)) to be solved in each step.

$$\frac{d^2}{dx^2}\left(EI\frac{d^2\omega}{dx^2}\right) = q \tag{3.3}$$

In this equation ω is the beam deflection and q is the distributed load, E is the Young modulus and I is the second moment of area.

$$\boldsymbol{Ku} = \boldsymbol{f} \tag{3.4}$$

Now $\boldsymbol{K}$ is the rigidity matrix, $\boldsymbol{u}$ is the displacement vector and $\boldsymbol{f}$ is the source term, which contains the loads applied. Abaqus has a wide variety of finite elements, but for thin-walled stainless steel structures, shell elements (S4R and S3R with reduced integration) are usually employed for meshing purposes.

When no time dependent effects are involved in the structural behaviour, other root finding methods, apart from the Newton-Raphson method, can be used to obtain the post-critical response of the structure; one of them is the arc-length method which is also included in the software Abaqus.

Second order geometric effects

For sway structures or slender members, the second order geometric effects of the loads applied have to be considered according to the EN 1993-1-1 [39]. This is done by finding the equilibrium between internal and external forces in the deformed shape of the structure.

For sway structures, an initial global geometric imperfection is needed to trigger, in some cases, the sway mechanism. For slender members, this initial imperfection also needs to be considered in order to trigger the out of plane deflections that are induced due to a buckling response.

In Abaqus the geometric imperfection can be introduced as an amplitude of a buckling mode of the structure. For not so advanced FE software it can be considered with an equivalent self-equilibrated load combination that reproduce the effect of the geometric imperfection. The amplitude of this geometric imperfection and the load values can be found in EN 1993-1-1 [39].

Residual stresses

Steel sections are usually rolled at elevated temperatures, exploiting its reduced mechanical properties to shape it easily. But, afterwards, a nonuniform cooling of the section induces residual stresses in the cross-section (see Figure 3.1). These residual stresses cannot be negligible when assessing the real behaviour of a structure at room temperature.

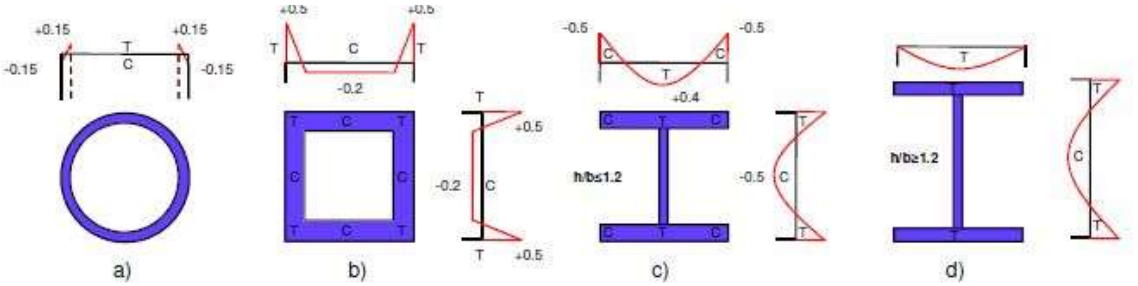

Figure 3.1: Residual stresses distribution depending on the section type. Values presented in terms of the yield stress.

Consequently, these residual stresses are usually introduced in the numerical model as an initial stress field along the members of the structure as shown in Figure 3.1.

Material modelling

Material mechanical properties are obtained from experimental tests and are included in European codes, as in EN 1993-1-2 [21], but these material properties are obtained by a tensile test which do not consider the phenomenon known as necking. The stress-strain relationship obtained in an experimental test is known as engineering or nominal stresses and are the ones provided in all codes.

For this reason, when assessing the real response of the structure by means of numerical models the material properties need to be modified into true stresses (see Eq. (3.5)).

$$\sigma_{true} = \sigma_{nom}(1 + \varepsilon_{nom})$$
$$\varepsilon_{ln}^{p} = ln(1 + \varepsilon_{nom}) - \frac{\sigma_{true}}{E} \tag{3.5}$$

This reformulation of the stress-strain relationship considers the effect of necking in the material response.

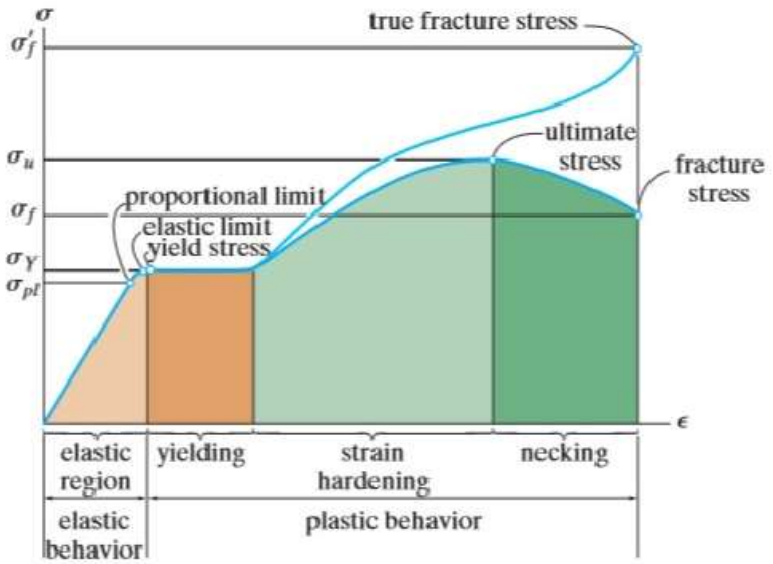

Figure 3.2: Nominal and true stress strain relationship for ductile materials [40].

Thermo-mechanical coupled problem

The thermo-mechanical coupled problem consists in solving the mechanical and the thermal problem at the same time. By doing so, the mechanical response is directly affected by the heat transfer problem and vice versa. Eq. (3.6) describes how the thermo-mechanical coupled problem is solved by means of incremental steps

$$\begin{bmatrix} \boldsymbol{K_{uu}} & \boldsymbol{K_{u\theta}} \\ \boldsymbol{K_{\theta u}} & \boldsymbol{K_{\theta\theta}} \end{bmatrix} \begin{Bmatrix} \Delta \boldsymbol{u} \\ \Delta \boldsymbol{\theta} \end{Bmatrix} = \begin{Bmatrix} \boldsymbol{R_u} \\ \boldsymbol{R_\theta} \end{Bmatrix} \tag{3.6}$$

where $\boldsymbol{K_{uu}}$ and $\boldsymbol{K_{\theta\theta}}$ are the stiffness matrices of the mechanical and thermal problem respectively, $\boldsymbol{K_{u\theta}}$ and $\boldsymbol{K_{\theta u}}$ represent how the mechanical problem affects the thermal problem and vice versa, $\Delta\boldsymbol{u}$ and $\Delta\boldsymbol{\theta}$ are the displacement and thermal increment vector and $\boldsymbol{R_u}$ and $\boldsymbol{R_\theta}$ are the error obtained in the last converged step.

As this problem includes time dependent effects the root finding method to be used is the Newton-Raphson method with load increments, which is not able to model the post-critical response of the structure. Numerical damping is also used to reduce the number of iterations needed to converge at each step. Additionally, it has been seen that numerical models that include numerical damping are able to describe the structure response just before collapsing better than modes without considering it.

A specific finite element that combines all degrees of freedom (mechanical and thermal) can be used for discretization purposes. Abaqus provides a finite element with thermal and mechanical degrees of freedom (S4RT and S3RT) that is used for thermo-mechanical coupled problems.

3.2 VALIDATION OF THE NUMERICAL MODEL

In order to prove that the numerical models used to assess the structural response of frames under fire conditions are trustworthy, different numerical and experimental tests from the literature will be reproduce using the software Abaqus. From simple to more complex problems involving nonlinear material effects, second order effects and thermo-mechanical coupled structural response are considered for the validation of the numerical model.

Thermal expansion effect

Thermal expansion plays a major role in the response of statically indeterminated structures under fire. The thermal elongation of a structure subjected to a temperature increment can be calculated as shown in Eq. (3.7).

$$\frac{dL}{L} = \alpha(T) \cdot \Delta T \tag{3.7}$$

Where $\frac{dl}{l}$ is the thermal elongation per unit of length, ΔT the temperature increment and $\alpha(T)$ is thermal elongation coefficient, which is temperature dependent. But, for simplified calculations, the thermal elongation can be assumed to be constant $\alpha = 1.2 \cdot 10^{-5} ^{\circ}\mathrm{C}^{-1}$.

When the Fourier's heat transfer equation (Eq. (2.16)) is solved, in the first time increments the temperature distribution depicts a parabolic curve, which as time passes becomes a linear distribution with a uniform slope along the element. In order to prove that the correct response of a beam subjected to a nonuniform temperature distribution can be obtained by means of numerical methods, a simply supported beam with a constant parabolic temperature distribution along it, presented in Figure 3.3, has been numerically modelled. The results derived from the numerical model are compared to analytical calculations.

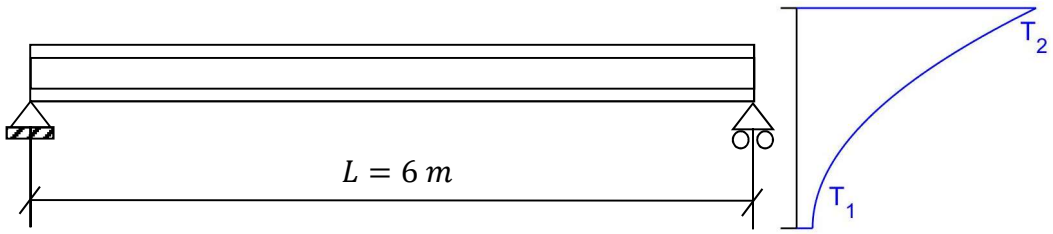

Figure 3.3: Representation of a simply supported beam with a parabolic temperature distribution.

Being the temperature at the lower fibre $T_1 = 15℃$ and at the upper fibre $T_2 = 30℃$ the temperature distribution can be described according to Eq. (3.8).

$$T(z) = 15 \cdot [1 + \left(\frac{z}{300}\right)^2] \tag{3.8}$$

This temperature distribution can be divided into a sum of three equivalent temperature distributions: a uniform temperature equal to the average temperature T_a of the section (zero order moment), a linear temperature distribution with a first order moment equal to the original temperature distribution, and a parabolic distribution with null resultant internal forces.

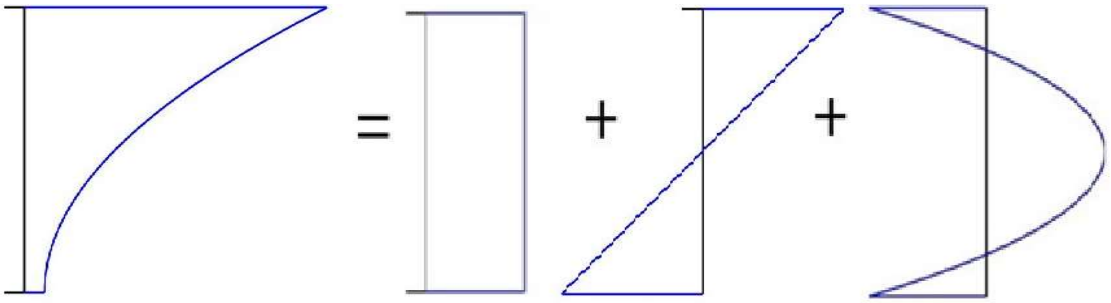

Figure 3.4: Temperature distribution decomposed into uniform, linear and parabolic temperature distributions.

The uniform distribution induces axial deformation, the linear temperature distribution induces uniform curvature along the beam and the parabolic temperature distribution describes the self-equilibrated stress distribution in each section in order to fulfil the Euler-Bernoulli theorem.

Defining the cross section as an IPE 300 without internal radius ($I_y = 7999\ cm^4$) and the material as a carbon steel S275 ($E = 210GPa$), the axial elongation and the maximum deflection can be analytically calculated.

$$dL = T_a \cdot \alpha \cdot L = 1.53\ mm \tag{3.9}$$

$$f_{max} = \frac{\chi \cdot l^2}{8} = 2.7\ mm \tag{3.10}$$

The results obtained by means of the FE model are $dL = 1.53\ mm$ and $\mathrm{f_{max}} = 2.7\ mm$, equal to the analytical results. Furthermore, the stress distribution in each section can be analytically obtain and it is shown in Figure 3.5. The same results are obtained from the numerical model (see Figure 3.6). FE model are in very good agreement with analytical results.

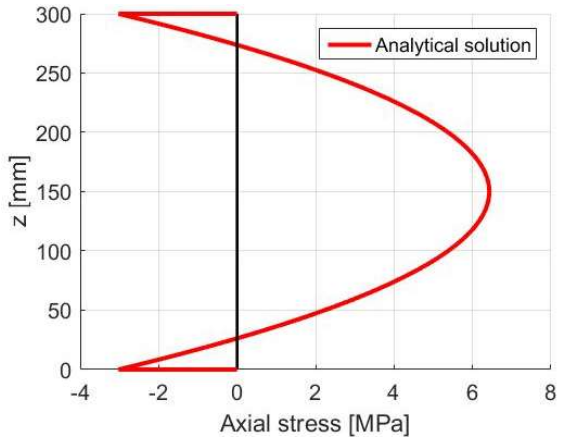

Figure 3.5: Analytical stress distribution.

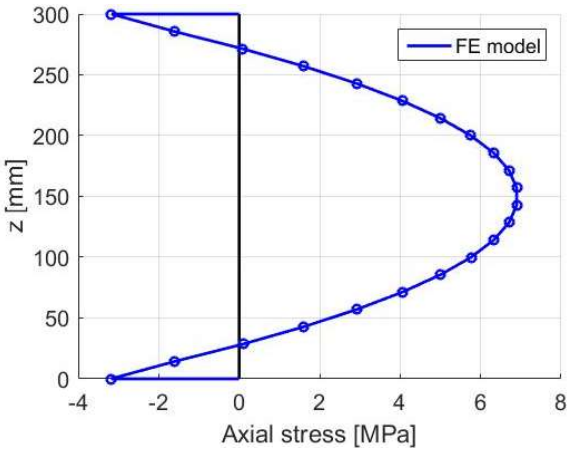

Figure 3.6: Stress distribution obtained by means of the numerical model.

Temperature development of a steel member subjected to fire

International codes provide simplified methods to assess the temperature of steel sections when being subjected to fire. These simplified methods assume a constant temperature for the whole cross-section.

Aiming for a good model calibration the temperature development of a circular steel section subjected to fire will be calculated by means of a finite element thermal analysis and validated against the temperature development analytically calculated according to the simplified method provided in EN 1993-1-2 [21].

For both cases it is assumed a uniform gas temperature in the chamber, therefore the ISO 834 is used in both cases. EN 1993-1-2 [21] inform about time step dependence of the simplified model and recommends time increments below 5 seconds.

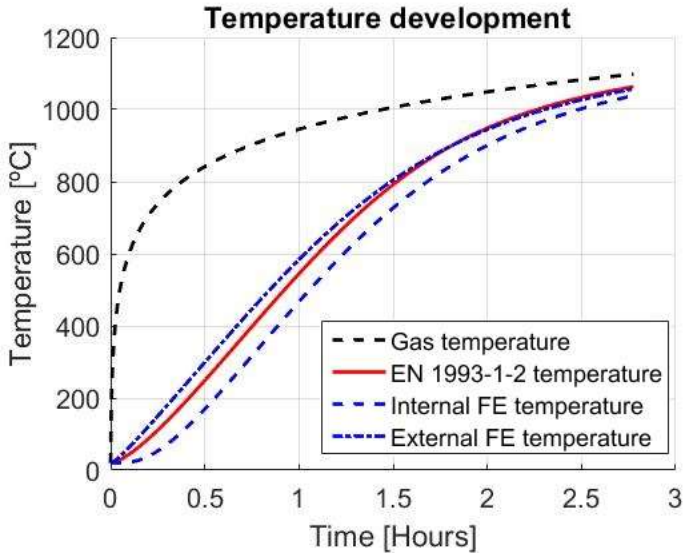

Figure 3.7: Temperature development of circular solid (diameter of 300 mm) carbon steel section.

As it can be seen in Figure 3.7, the simplified method included in EN 1993-1-2 [21] is a good approximation of the temperature development for carbon steel members, but a temperature gradient within the steel section is noted and is not considered in the simplified method. In addition, no step size dependence is detected in the FE model.

Nonlinear material response due to temperature increase

Gillie [41] presents a problem that can be reproduced to calibrate numerical models involving a decrease of mechanical properties due to a temperature increase. Moreover, this numerical problem also assesses the effect of the thermal expansion in beams depending on the boundary conditions.

The problem to be reproduced is a simply supported beam subjected to distributed load, assessing the response of the beam when it is subjected to a temperature increase and subsequently cooled to room temperature (see Figure 3.8). Additionally, the same problem will be analysed varying the supports stiffness.

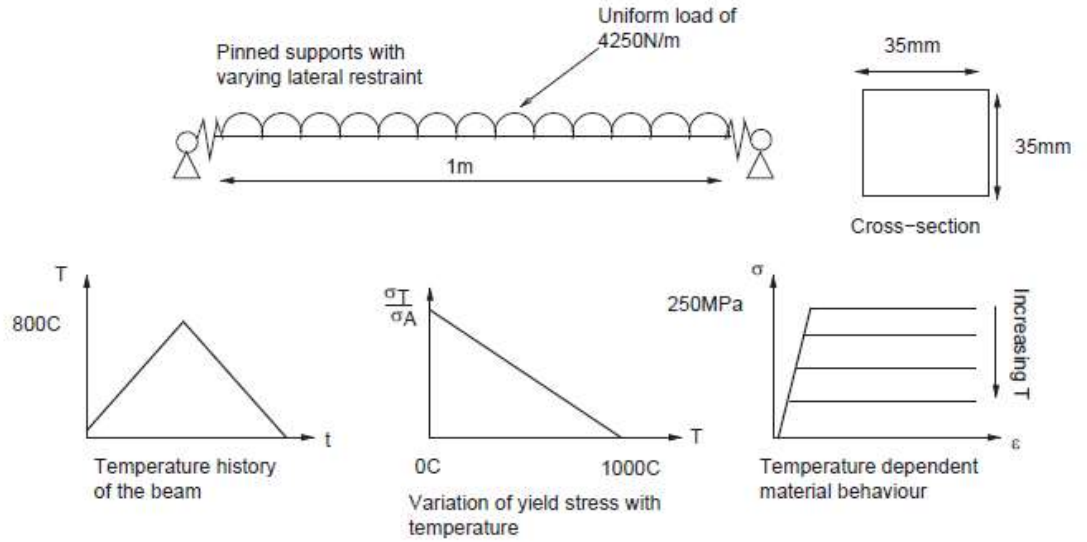

Figure 3.8: Main parameters of the problem of the defined problem [41].

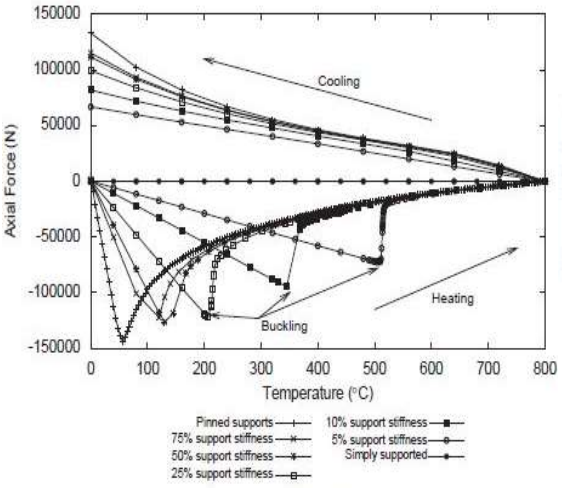

Figure 3.9: Axial force predicted by a materially and geometrically non-linear analysis [41].

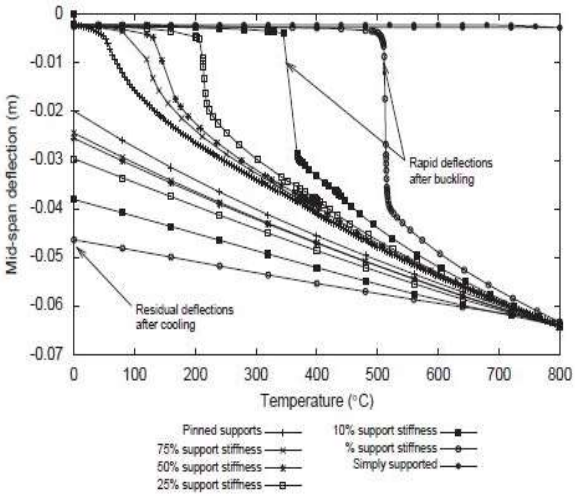

Figure 3.10: Deflections predicted by a materially and geometrically non-linear analysis [41].

Figure 3.9 and Figure 3.10 describe the response of the beam subjected to a temperature increase and a subsequent temperature decrease. The rate of increase of the axial force is directly related to the stiffness of the supports. The maximum axial force is obtained just before buckling occurs, therefore large deflections are produced. As a consequence of it most of the thermal expansion is released by geometric lengthened of the beam, resulting in a reduction of the axial force. The large curvature of the beam induces plastic deformations that after cooling produces residual deflections and residual stresses.

Figures 3.11 and 3.12 show the results obtained using the numerical model and show total agreement with the results presented by Gillie [41].

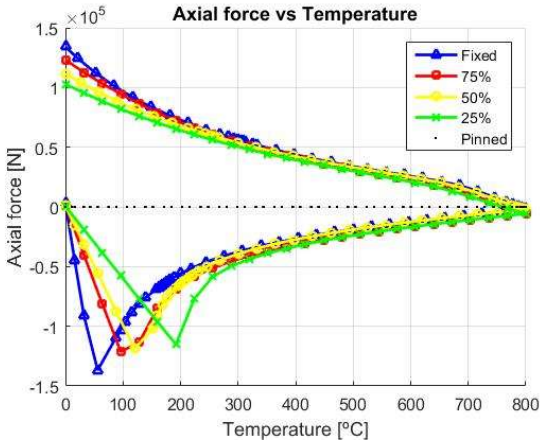

Figure 3.11: Axial force development under a cycle of temperature increase and decrease of the beam.

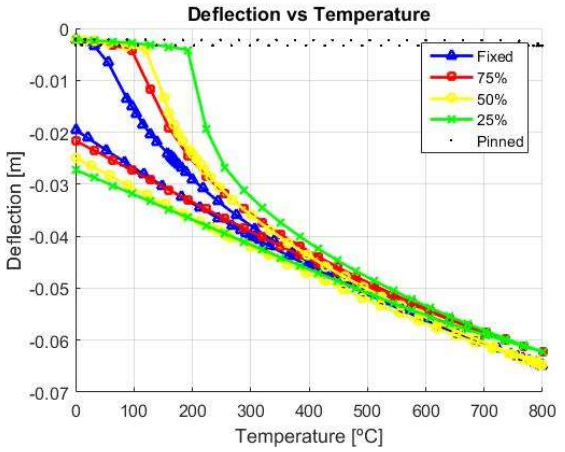

Figure 3.12: Deflection development under a cycle of temperature increase and decrease of the beam.

Isothermal numerical test reproduction. Lateral torsional buckling

Buckling failure is characterized by an abrupt collapse with little advise before reaching the critical load, consequently it must to be avoided. For this reason, assessing the effect of global buckling is vital in order to correctly design steel members.

The main problem with global buckling under fire situation is that a well-designed member at room temperature may suffer from buckling at elevated temperatures when its mechanical properties are reduced. For this reason, there are specific χ-$\bar{\lambda}$ diagrams presented in EN 1993-1-2 for fire situations, which are based on multiple parametric studies of carbon steel members tests.

In order to assess the numerical model, one of these isothermal numerical tests presented by Vila Real et al. [42] have been reproduced. The research group of the University of Aveiro modelled the behaviour of a simply supported beam with fork supports subjected to an isothermal test at $500℃$ with the FE software Safir. The authors discretized the structure using beam elements (linear elements), so no local effects were considered.

The objective of the numerical test is to determine the critical load of the beam at $500℃$. Since the cross section is an open section IPE 220 made of stainless steel (grade 1.4301) is susceptible to lateral torsional buckling. Therefore, in order to trigger the buckling response of the structure in a numerical model, an initial geometric imperfection should be applied. The authors used a sinusoidal global imperfection with a midspan section

twist. However, initial geometric imperfection can also be an amplitude of a global eigenmode of the structure, obtained by means of an eigenvalue analysis (diagonalizing the stiffness matrix). The eigenmode shown in Figure 3.13 has been used as an initial geometric imperfection for the present study.

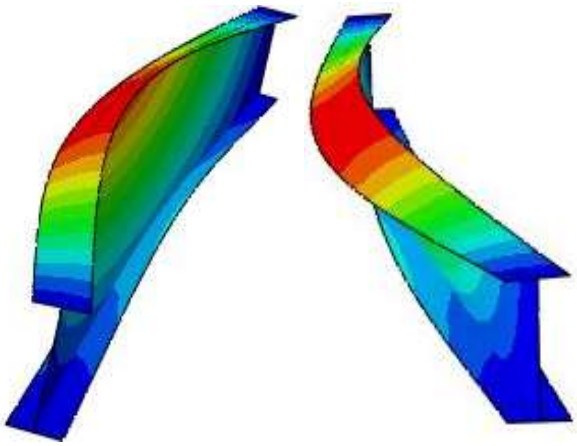

Figure 3.13: Two views of the first buckling mode of a I section subjected to a uniform distributed load. Used as an initial imperfection.

The original authors obtained a maximum distributed load of $q_{max} = 5.63\ \mathrm{kN/m}$ and provided the load vs midspan deflection diagram (see Figure 3.14).

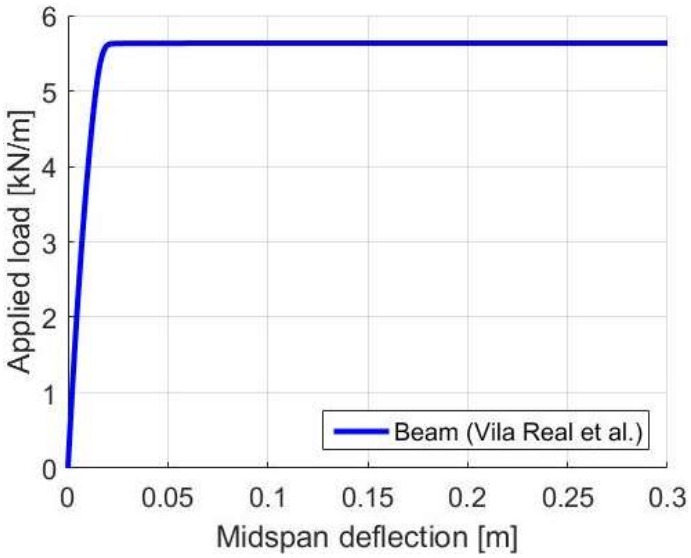

Figure 3.14: Load-deflection curve obtained by the authors (Vila Real et al. [42]).

As it can be seen, the numerical test from the paper present a horizontal platoon after reaching the critical load, even though, problems considering nonlinear material and second order geometrical effects are known to show a load decrease after reaching the critical load [43].

In order to reproduce these results by means of Abaqus code, the beam has been discretised with beam elements (linear elements) and shell elements and both results have been compared to the original results.

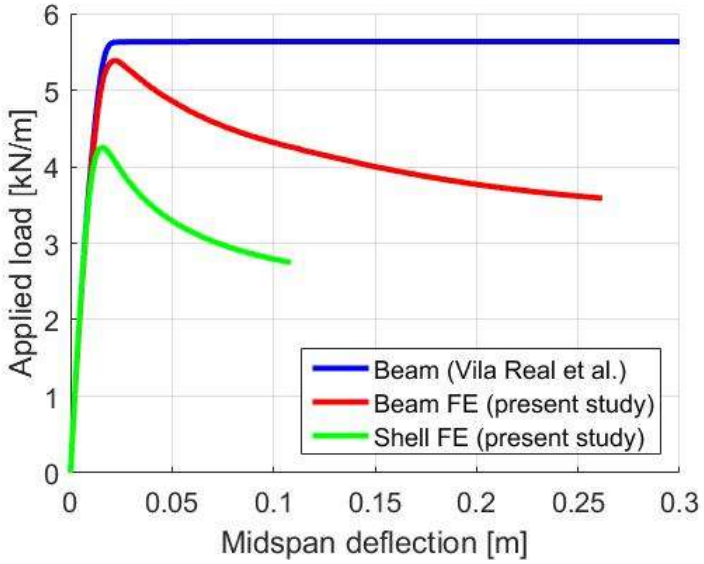

Figure 3.15: Load-deflection curves obtained by beam elements, shell elements and by the authors.

As it can be seen in Figure 3.15 the beam model, with $q_{max} = 5.38\ \mathrm{kN/m}$, shows a reasonable agreement with the results presented by the original authors, whereas the shell model, with $q_{max} = 4.25\ \mathrm{kN/m}$, shows a 21% decrease of the maximum load. The reason behind this is further explained in Walport et al [44], but it is mainly due to local effects that cannot be reproduced using beam elements. This behaviour is even observed for Class 1 cross-sections.

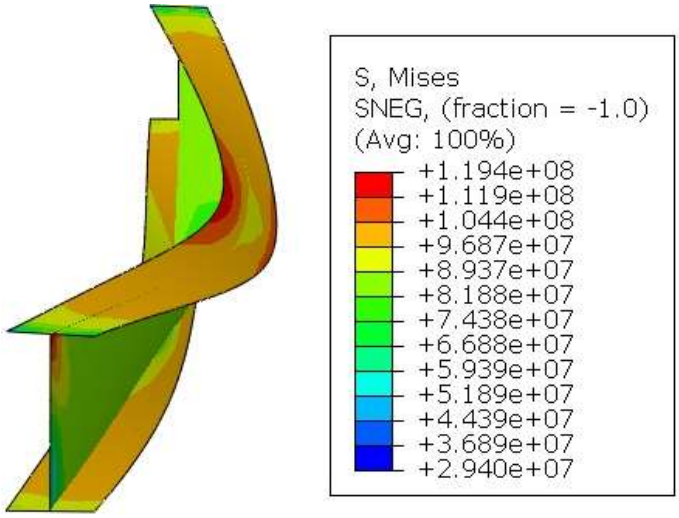

Figure 3.16: Von Misses stress distribution (N/m^2) of the beam showing a lateral torsional buckling response.

Figure 3.16 shows the response of the beam discretized with shell elements under the applied loads, describing a torsional-lateral buckling failure.

Anisothermal laboratory test reproduction

The most common stainless steel sections used in construction are the cold-formed hollow sections. This type of section is not susceptible to torsional lateral buckling but to flexural buckling. With the objective to calibrate the numerical model, the response of a hollow section column (80x80x3x2500mm) is numerically reproduced. This column was tested in the University of Liège by Rossi [45] and it was afterwards used as a benchmark by Afshan in her PhD thesis [46].

This anisothermal test subjected the column to fire (ISO 834) in its 4 sides while a constant axial load was applied, increasing the temperature until failure. The goal of this test was to obtain the critical temperature and consequently the time resistance of the member.

The test specimen was fixed at both ends to prevent cross-sectional deformation, lateral displacements, rotations and warping. The load applied $78\ \mathrm{kN}$, was the equivalent load corresponding to a degree of utilization $\mu_0 = 0.3$,.

Figure 3.17: Different points of view of the column after the laboratory test [45].

Local buckling and global buckling were observed in the laboratory tests, for this reason a local and global geometric imperfection were introduced in the numerical model. Figure 3.18 shows the deformed shape of the specimen obtained by means of numerical model.

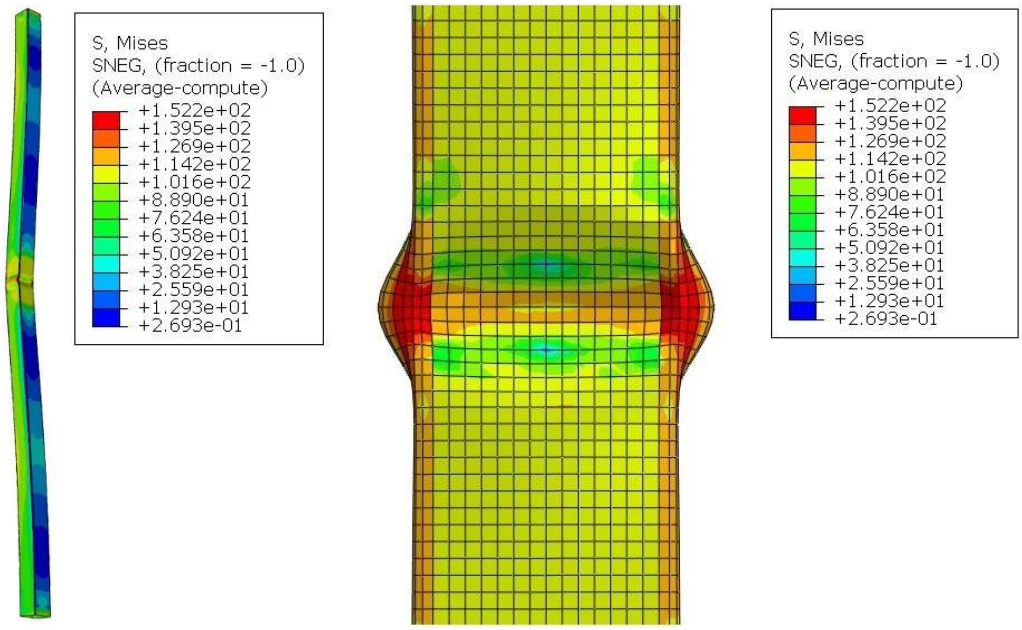

Figure 3.18: Von Mises stress (N/m^2) distribution before failure obtained by means of the FE model.

Good agreement can be observed between experimental and numerical results. On the other hand, the FE model predicted a critical furnace temperature of 712℃, whereas the critical furnace temperature derived from the experimental results was 708℃. Additionally, the critical specimen temperature derived from the numerical model was 681℃.

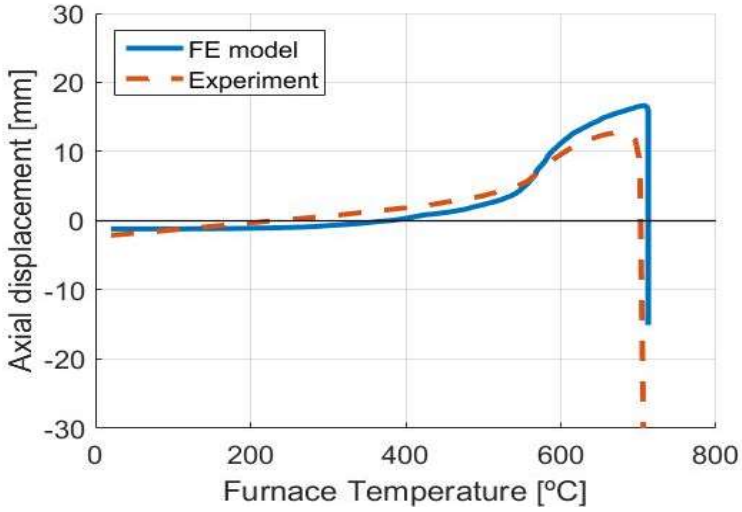

Figure 3.19: Axial displacement versus furnace temperature curve obtained in the laboratory test and by means of the FE model.

3.3 HEAT TRANSFER MODEL FOR HOLLOW SECTIONS

As it has already been mentioned, cold formed hollow sections are the main stainless steel sections used for building construction. It seems to be clear that, when this type of

section is subjected to fire, heat flux exists inside the cavity, transferring heat from hotter parts to colder parts. In such narrow cavities without openings, fluid movement is very limited, consequently convective heat transfer becomes insignificant. Therefore, radiative heat transfer becomes the main source of heat transfer inside the cavity.

Introduction to the simplified model

In order to model this phenomenon, a simplified numerical method has been developed to assess the temperature development of the air inside the cavity. This model assumes that the gas temperature along the cavity is uniform, thus the gas temperature development over time can be obtained solving the heat transfer problem within the cross-section. Additionally, the conductive heat transfer has been simplified in the model, modelling the heat flux between adjacent steel faces.

In order to formulate and solve the heat transfer problem the cross-section geometru and the heat transfer problem have been simplified as explained below:

1. Each steel face is modelled as a constant steel volume with a uniform temperature.
2. The air temperature is assumed to be uniform.
3. The thermal properties of steel and air are calculated at each time increment. Steel properties have been obtained from EN 1993-1-2 [21], whereas air thermal properties from Çegel and Cimbala [47].
4. Conductive heat flux is calculated at each time increment between adjacent steel faces with the following expression

$$q_{cond,ij} = \frac{\lambda_i + \lambda_j}{2} \cdot \frac{T_i - T_j}{d_{ij}} \tag{3.11}$$

   where λ_i is the conductivity, T_i is the temperature and d_{ij} is the distance between the centres of gravity of two adjacent steel volumes.
5. Heat transfer between steel faces and external air considers radiative heat flux and convective heat flux. External gas temperature is prescribed with a normalized curve, for instance the ISO 834 curve.
6. The temperature increment for each steel volume is calculated as shown in Eq. (3.12) and the gas temperature increment as described in Eq. (3.13).

$$\Delta T_{s,i} = \frac{Q_{int,i} + Q_{ext,i} + \sum_j Q_{cond,i-j}}{\alpha_{s,i} \cdot V_{s,i} \cdot \rho_s} \cdot \Delta t \tag{3.12}$$

$$\Delta T_g = \frac{\sum_i Q_{int,i} + Q_{ext,i}}{\alpha_g \cdot V_g \cdot \rho_g} \cdot \Delta t \tag{3.13}$$

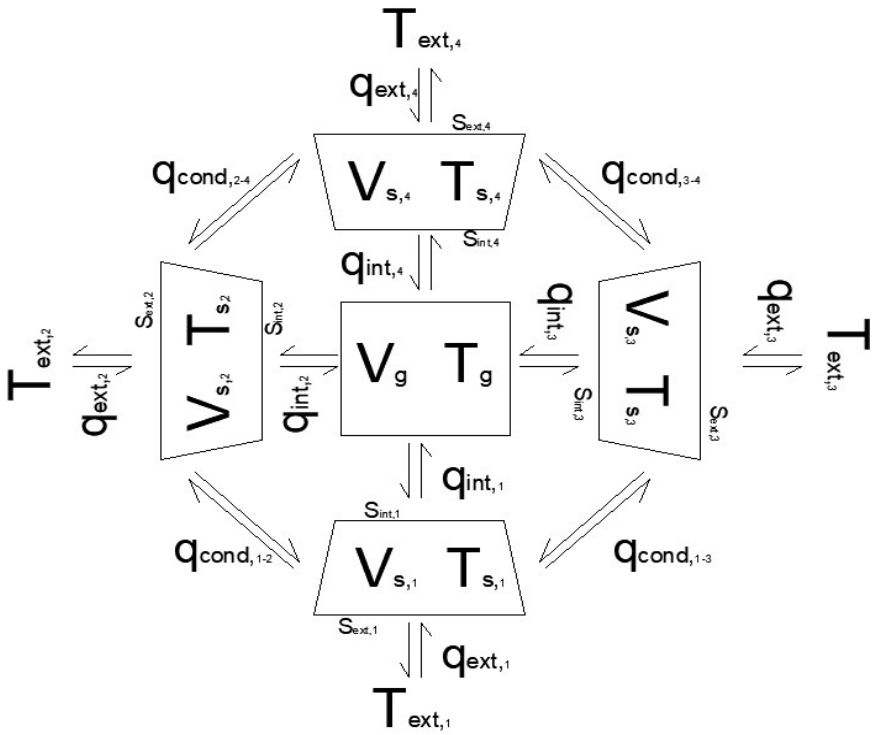

Figure 3.20: Cavity gas temperature developed model.

With this simplified model the cavity gas temperature development over time can be calculated (see Figure 3.20). Then it can be prescribed as a surface condition in the FE model where the thermo-mechanical coupled problem is solved.

Modelling of cavity radiation in Abaqus

Abaqus includes a specific boundary condition for this type of problems, called cavity radiation [38]. This boundary condition needs to be applied on the surfaces that are in contact with the cavity radiation. The Abaqus code calculates the so-called view factors, that takes into consideration the cavity geometry, and solves the cavity heat transfer problem. Unfortunately, this surface condition cannot be applied in problems where deflections are involved, such as in thermo-mechanical coupled problems. It could be used in a sequentially thermo-mechanical problem, where the thermal problem is solved first and then implemented in the nonlinear mechanical problem as a

temperature field, but this method can only be implemented in cavities with less than 16000 nodes, which limits the mesh size of the model.

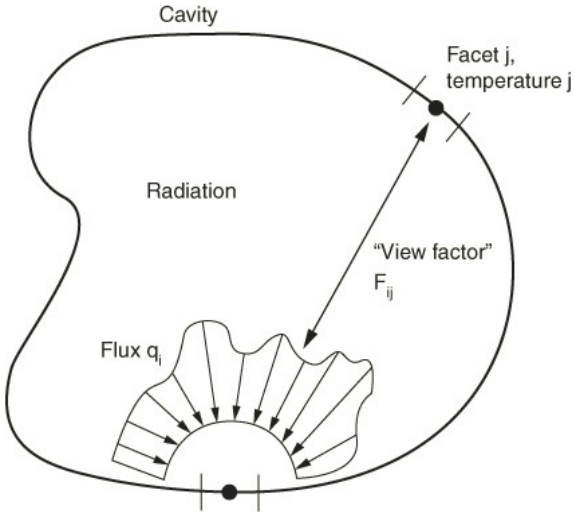

Figure 3.21: Cavity radiation problem, considering the view factor. [38].

Nonetheless, Abaqus is offering a simplified method to consider the heat transfer inside a cavity [38]. This method can be used in thermo-mechanical coupled problems, but consider the cavity as a black body (emissivity equal to 1) and considers its temperature as the average over the cavity surface. Then, the radiation heat flux in each facet is calculated considering its surface area and the emissivity defined.

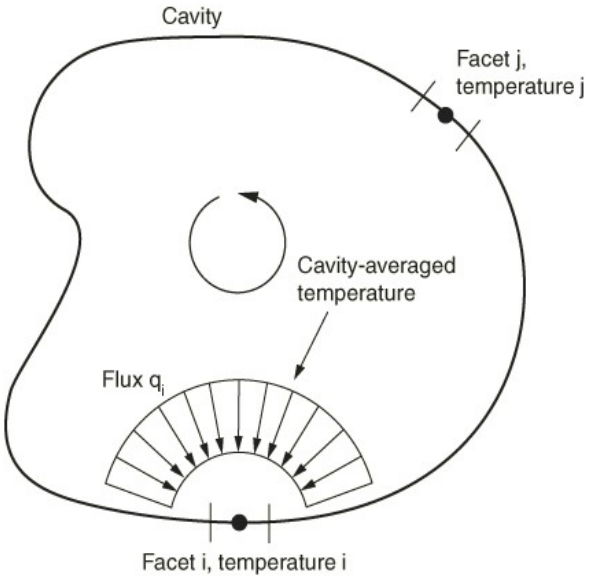

Figure 3.22: Approximate method for cavity radiation included in Abaqus [38].

Calibration of the simplified cavity radiation model

In order to assess the reliability of the proposed model, a thermo-mechanical coupled problem is presented (see Figure 3.23) where the cavity heat transfer may have a significant impact in the structural response of an austenitic stainless steel (1.4301) column.

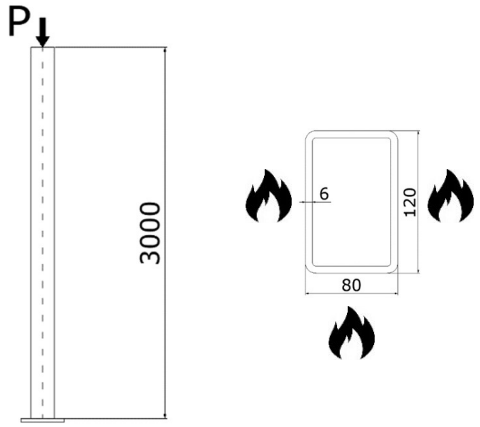

Figure 3.23: Column geometry (mm) and loads applied under fire situation.

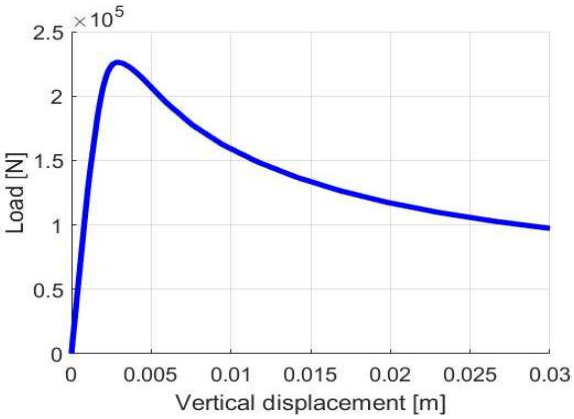

Figure 3.24: Load-displacement curve of an 80×120×6 RHS column.

The design load applied is the corresponding load to a degree of utilization of $\mu_0 = 0.4$, the ultimate load $R_{fi,d,0}$ at room temperature has been obtained by means of a FE model and it is assumed as the peak load of the load-displacement curve ($226.183\ \mathrm{kN}$) (see Figure 3.24). Consequently, for the thermo-mechanical coupled analysis an initial step at room temperature has been defined, where the initial load is applied ($90.473\ \mathrm{kN}$). Subsequently, the fire step is defined. In this step three external faces of each section are heated up according to the ISO 834 curve, leaving the other external face in contact with the outside air, permanently at $20℃$. The inner faces of each section are in contact to the cavity air. The fire step lasts until failure of the analysed column.

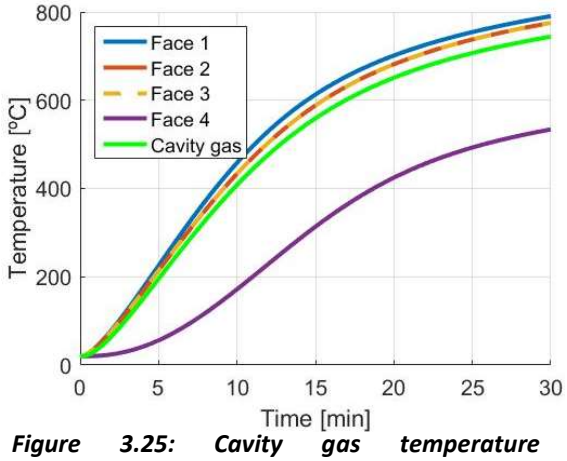

Figure 3.25: Cavity gas temperature development obtained from the proposed numerical model.

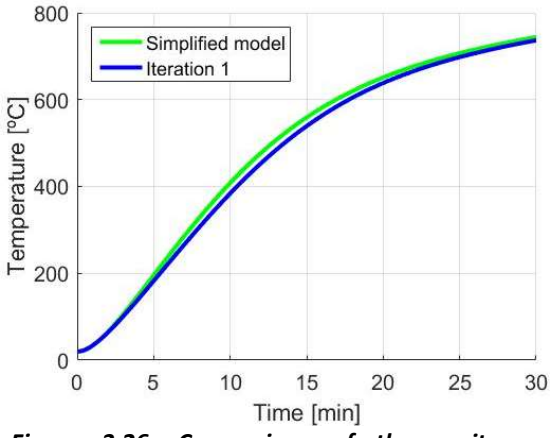

Figure 3.26: Comparison of the cavity gas temperature obtained from the proposed numerical model and after the first iteration.

Figure 3.25 shows the cavity gas temperature calculated by means of the proposed model and the computed temperatures for the steel faces of the analysed section. This cavity gas temperature has been introduced as a surface boundary condition in the Abaqus model. From the thermo-mechanical coupled analysis carried out in Abaqus the temperature of each steel face can be obtained again. Then, the cavity gas temperature can be recalculated with the temperatures extracted from the FE model. This process should be done iteratively until the gas temperature curve introduced for the thermo-mechanical problem and the cavity gas temperature curve derived from the numerical model are in good agreement. Fortunately, after one iteration both temperature gas curves show good agreement (see Figure 3.26).

Furthermore, the presented problem is solved by 3 different FE models: considering no radiative heat flux in the cavity (*NoRad*), considering the cavity radiation using the simplified cavity radiation condition included in Abaqus (*Abaqus*) and prescribing the cavity gas temperature obtained from the proposed model (*Model*). A previous thermal analysis of the column has been carried out and the temperature development of a steel section of the column is obtained by these 3 FE models and presented in Figure 3.27.

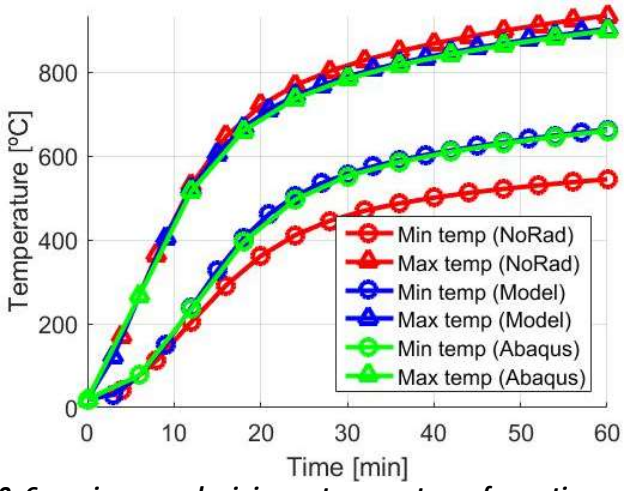

Figure 3.27: RHS 80×120×6 maximum and minimum temperature of a section over time.

As it can be seen, the model without cavity radiation exhibits a higher temperature gradient, whereas both models that consider cavity radiation lead to smaller temperature gradient and show good agreement between them. Temperature gradient induces thermal curvature, thus models with reduced temperature gradient are in a better position in terms of mechanical response (see Figure 3.27).

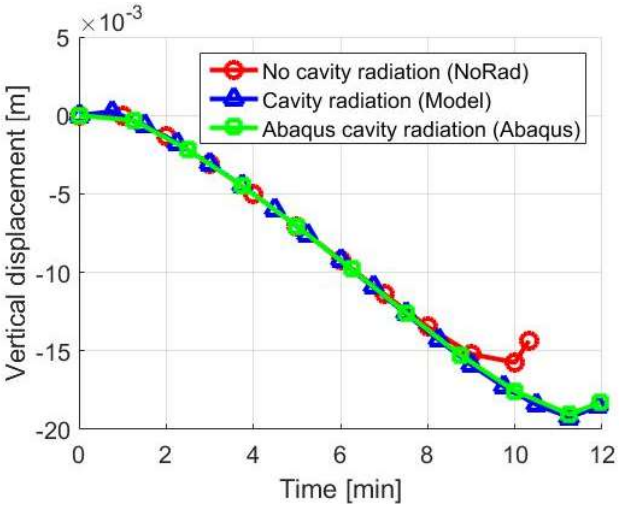

Figure 3.28: Vertical displacement over time of the 3 FE models.

Figure 3.28 shows the column vertical displacement over time, considering column expansion as negative vertical displacement. Models that consider cavity radiation exhibit higher time resistance (see Table 3.1), proving that in order to correctly model the structural response of steel structures under fire, cavity radiation cannot be neglected. Moreover, both FE models that consider cavity radiation show good agreement, thus both ways of modelling cavity radiation can be implemented in further models.

	No radiation	Simplified cavity radiation model	Abaqus simplified cavity radiation
Time resistance	10.3 min	11.9 min	12 min

Table 3.1: Time resistance obtained by different numerical models of the RHS 80×120×6 column subjected to fire.

CHAPTER 4

4. STUDY OF THE RESPONSE OF STAINLESS STEEL FRAMES UNDER FIRE

4.1 BASIS FOR THE STUDY

In recent years, a considerable amount of research has been devoted to the structural analysis and design of isolated stainless steel members at elevated temperatures. However, advances related to the behaviour of stainless steel frames subjected to fire are scarce. Actually, EN 1993-1-4 [17] does not provide design rules for the analysis of stainless steel structures under fire situation and EN 1993-1-2 [21] provides a conservative approach for the fire design based on carbon steel tests.

For these reasons, the same stainless steel frame (see Figure 4.1) is analysed varying the boundary conditions, the material and the degree of utilization (load applied) with the objective of assessing the response of a stainless steel frames subjected to fire and trying to identify key factor that rule their behaviour under fire.

Stainless steel frame design

The frame to be numerically analysed under fire is an austenitic stainless steel (1.4301) non-sway frame with fixed supports. The cross section is an 80×120×6mm rectangular

hollow section, constant along the frame. It is a Class 1 section, meaning that it can form plastic hinges with the rotation capacity required to form a plastic mechanism. The frame geometry and cross-section are the same that one of the frames that were mechanically tested in the Laboratory of Structures and Materials "Lluis Agulló" in the UPC, presented in Arrayago et al. [48].

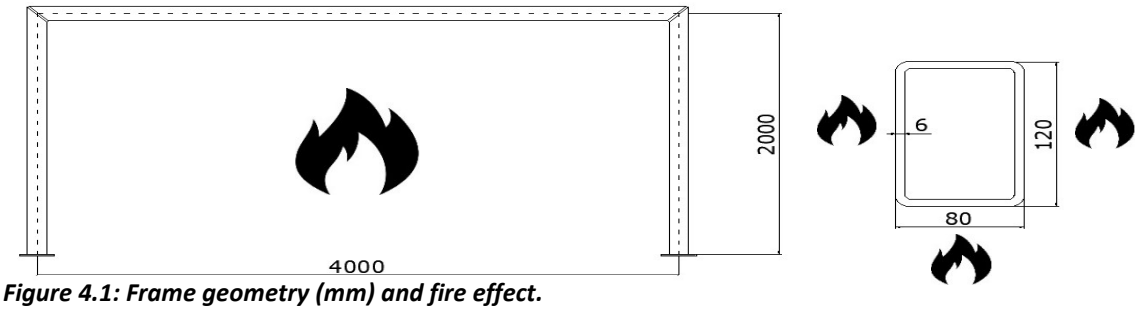

Figure 4.1: Frame geometry (mm) and fire effect.

The three inner faces of each section are heated up according to the ISO 834 curve, leaving the outer face in contact with the outside air, permanently at 20℃. Cavity radiation is also considered in the numerical model.

Material definition

The austenitic stainless steel (1.4301) is one of the most common stainless steel used in construction. For this reason, it has been used as the frame material and its stress-strain relationship has been defined according to EN 1993-1-2, Annex C [21] (see Figure 4.2). Additionally, the reduction coefficients are presented in Table 4.1.

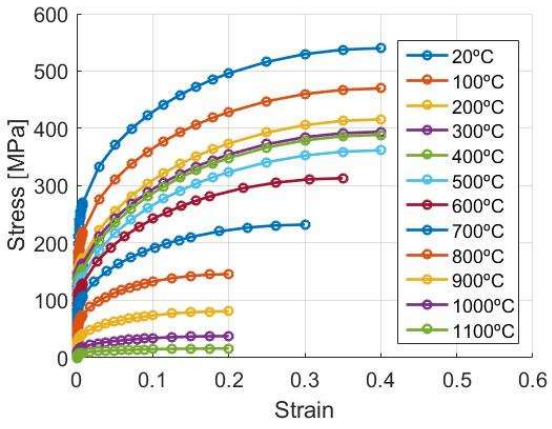

Figure 4.2: Austenitic (1.4301) stress-strain relationship according to the EN 1993-1-2 [21].

Temperature	k_E	$k_{f_{0.2}}$	k_{f_u}
20℃	1	1	1
100℃	0.96	0.82	0.87
200℃	0.92	0.68	0.77
300℃	0.88	0.64	0.73
400℃	0.84	0.6	0.72
500℃	0.8	0.54	0.67
600℃	0.76	0.49	0.58
700℃	0.71	0.4	0.43
800℃	0.63	0.27	0.27
900℃	0.45	0.14	0.15
1000℃	0.2	0.06	0.07
1100℃	0.1	0.03	0.03
1200℃	0	0	0

Table 4.1: Austenitic (1.4301) reduction factors according to EN 1993-1-2 [21].

Combination of loads

The combination of loads applied has been designed in order to trigger a global failure mechanism of the fixed-fixed Class 1 frame. After analysing multiple combinations of loads and the corresponding failure mechanisms, the design loads are the following:

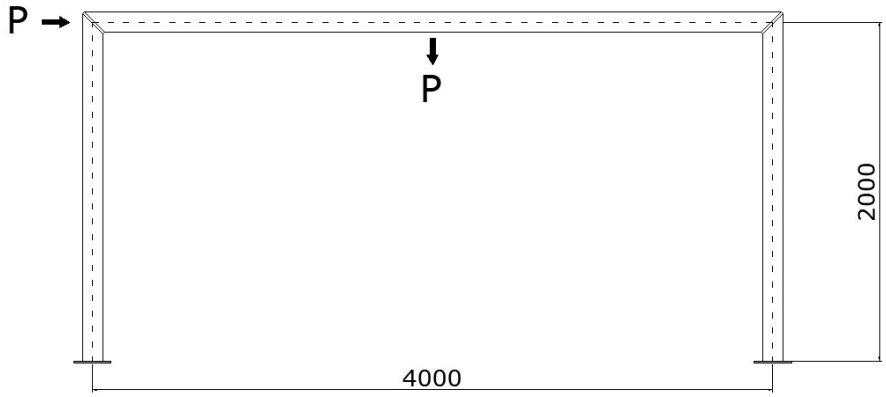

Figure 4.3: Frame geometry (mm) and loads applied of the Class 1 frame with fixed supports.

This combination of loads may trigger several failure mechanisms:

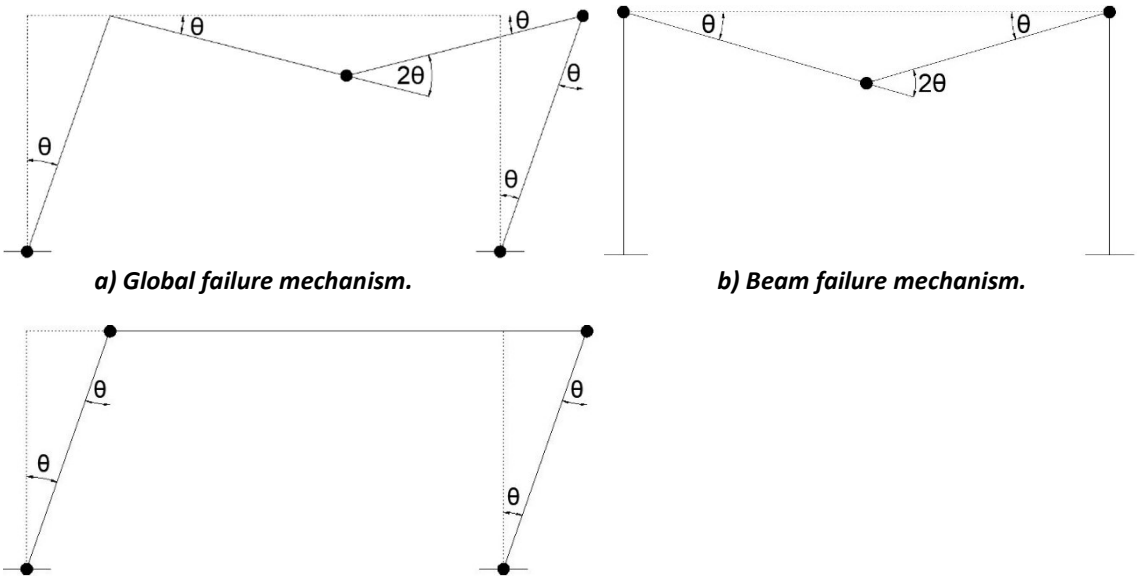

a) Global failure mechanism.

b) Beam failure mechanism.

c) Sway failure mechanism.

Figure 4.4: Possible failure mechanisms of a fixed-fixed frame under the loads applied.

Applying the principle of virtual work (Eq. (4.1)), the failure mechanism of the frame can be determined.

$$W_{ext} = \sum F_i \cdot \delta_i = \sum M_{pl,j}\theta_j = W_{int} \tag{4.1}$$

The load needed to trigger the global failure mechanism shown in Figure 4.4.a is

$$W_{int} = M_{pl}\theta + M_{pl}\theta + 2M_{pl}\theta + 2M_{pl}\theta = 6M_{pl}\theta \tag{4.2}$$

$$W_{ext} = P\delta_H + P\delta_V = 2Pl\theta \tag{4.3}$$

$$P = \frac{3M_{pl}}{l} \tag{4.4}$$

where l is the column height equal to half of the beam length and M_{pl} is the plastic bending moment. In the same way, the load needed to trigger the partial failure mechanism, described in Figure 4.4.b

$$W_{int} = M_{pl}\theta + M_{pl}\theta + 2M_{pl}\theta = 4M_{pl}\theta \tag{4.5}$$

$$W_{ext} = P\delta_V = Pl\theta \tag{4.6}$$

$$P = \frac{4M_{pl}}{l} \tag{4.7}$$

Finally, the load needed to trigger the sway failure mechanism shown in Figure 4.4.c can be obtained as before:

$$W_{int} = M_{pl}\theta + M_{pl}\theta + M_{pl}\theta + M_{pl}\theta = 4M_{pl}\theta \tag{4.8}$$

$$W_{ext} = P\delta_H = Pl\theta \tag{4.9}$$

$$P = \frac{4M_{pl}}{l} \tag{4.10}$$

Therefore, according to the rigid plastic analysis the failure mechanism that is expected to be described under the loads applied is the global failure mechanism, shown in Figure 4.4.a.

Initial geometric imperfection

As it has been introduced previously, initial geometric imperfections are needed in numerical model to trigger second order geometric effects, such as member buckling.

For the numerical model created to assess the behaviour of the frame presented in Figure 4.5 the initial geometric imperfection used will be the deformed shape of the first sway eigenmode.

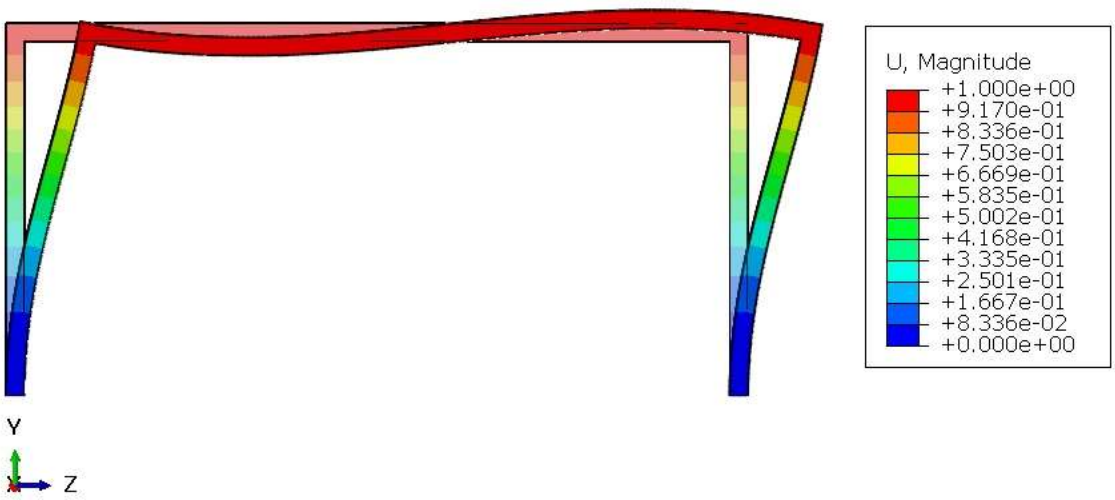

Figure 4.5: First sway eigenmode of a fixed-fixed frame. Displacement values are normalized.

The eigenmodes of a structure, and the associated eigenvalues, have been obtained by means of a buckling analysis, diagonalizing the stiffness matrix. For all the studied cases presented below the amplitude of the geometrical imperfection applied is $h/500$, being h the height of the columns.

Residual stresses

Even thought, residual stresses have a nonnegligible effect at room temperature, a study realized by Zhan el al. [49] proved that the effect of the residual stresses drastically vanishes at elevated temperatures.

For the studied case, all frames are subjected to fire, consequently they are expected to collapse at elevated temperatures, where residual stresses effects have been proved to vanish. Hence residual stresses have not been included in the numerical models.

4.2 AUSTENITIC STAINLESS STEEL FRAME RESPONSE UNDER FIRE

Structural response at room temperature

The ultimate load $R_{fi,d,0}$ at room temperature has been obtained by means of a FE model and it is assumed as the peak load of the load-displacement curves presented in Figure 4.6 and Figure 4.7. This peak load is 34.731 kN.

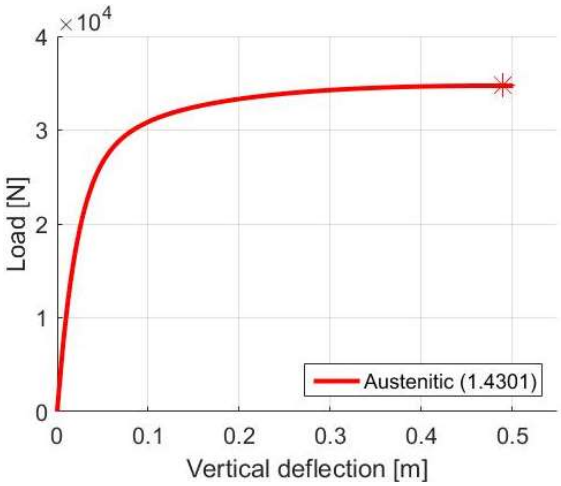

Figure 4.6: Load vs vertical displacement curve at room temperature.

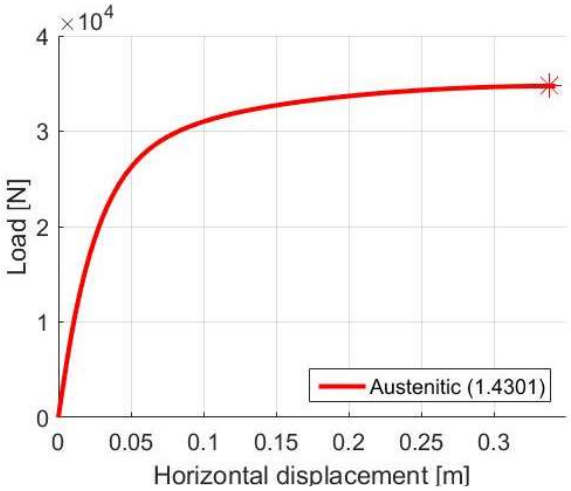

Figure 4.7: Load vs horizontal displacement curve at room temperature.

Since the critical load at room temperature has been obtained by means of a nonlinear material and geometric analysis, applying the vertical and horizontal load incrementally, plastic hinges will not be formed at the same time, but will be formed according to the bending moment distribution at each load increment.

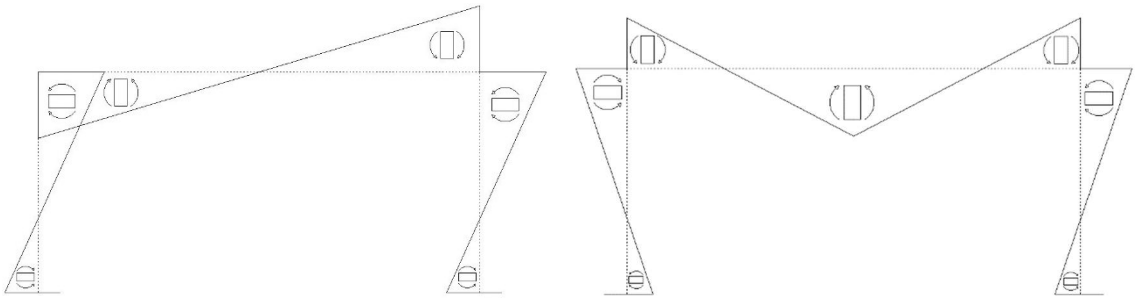

a) Horizontal load. ***b) Vertical load.***

Figure 4.8: Bending moment distribution under the applied loads.

As it can be seen in Figure 4.8, by means of a first order linear analysis, the maximum bending moment under this combination of loads appears in the top right joint. When this joint reaches the plastic bending moment, the further forces applied redistribute until all the plastic hinges needed to describe global failure mechanism are formed. The deformed shape of the frame when the ultimate load is applied is shown in Figure 4.9.

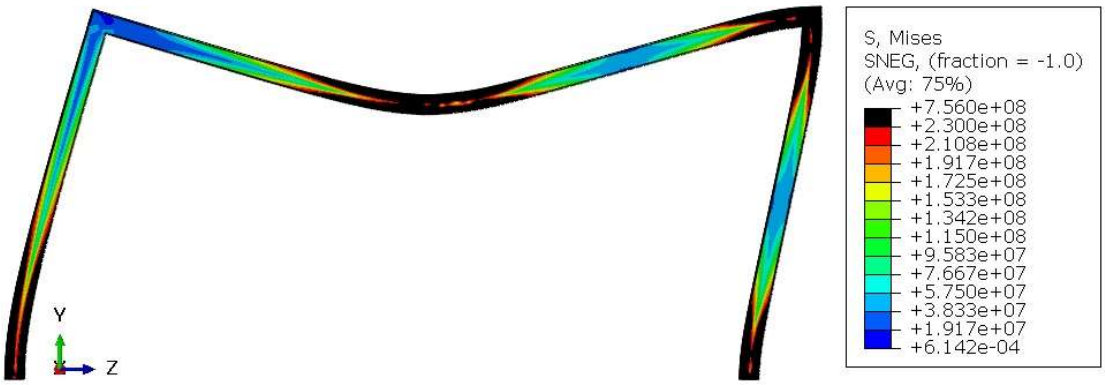

Figure 4.9: Von Misses stress distribution (N/m^2) of the austenitic (1.4301) frame under ultimate load (black regions are elements with stresses over the proof stress $f_{0.2}$).

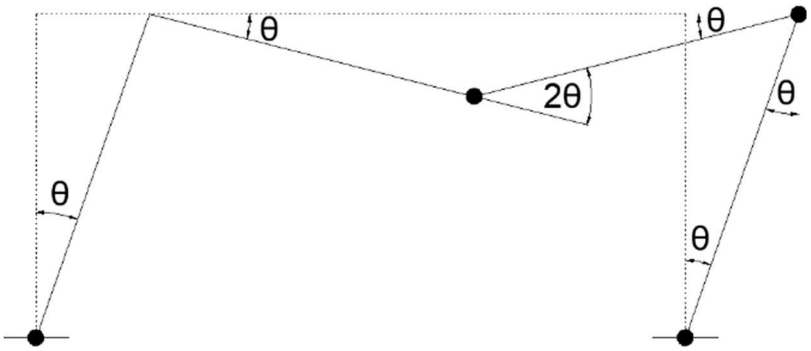

Figure 4.10: Theoretical global plastic mechanism of a fixed-fixed frame.

The deformed shape and the Von Misses stress distribution shown in Figure 4.9 are in good agreement with the theoretical global plastic mechanism derived from the application of the principle of virtual work (see Figure 4.10), proving that the design loads applied have fulfilled the design goal.

Thermo-mechanical coupled analysis

For the thermo-mechanical coupled analysis an initial load step at room temperature has been defined, where the initial load, corresponding to a degree of utilization $\mu_0 = 0.3$ $(10.419\ \mathrm{kN})$, is applied. Subsequently, a fire step is defined. In this step the three inner faces of each section are heated up according to the ISO 834 curve, leaving the outer face in contact with the outside air, permanently at $20℃$, and including cavity radiation. This fire step lasts until failure of the analysed frame.

Time resistance and critical temperatures for the studied case are shown in Table 4.2. Since temperature is not uniform along the frame because of the fire load, the inner and outer face mean temperature at failure are derived from the numerical model.

	Time resistance	Inner face mean temperature	Outer face mean temperature
Austenitic 1.4301	47.3 min	866°C	675°C

Table 4.2: Main results of the austenitic (1.4301) stainless steel frame subjected to fire.

The frame fails describing a global collapse mechanism and developing extensive plastics regions on both supports, on the midspan section of the beam and on the right joint. Beyond this fire load, internal forces cannot be further redistributed. Figure 4.11 shows the Von Mises stresses before failure according to the FE model.

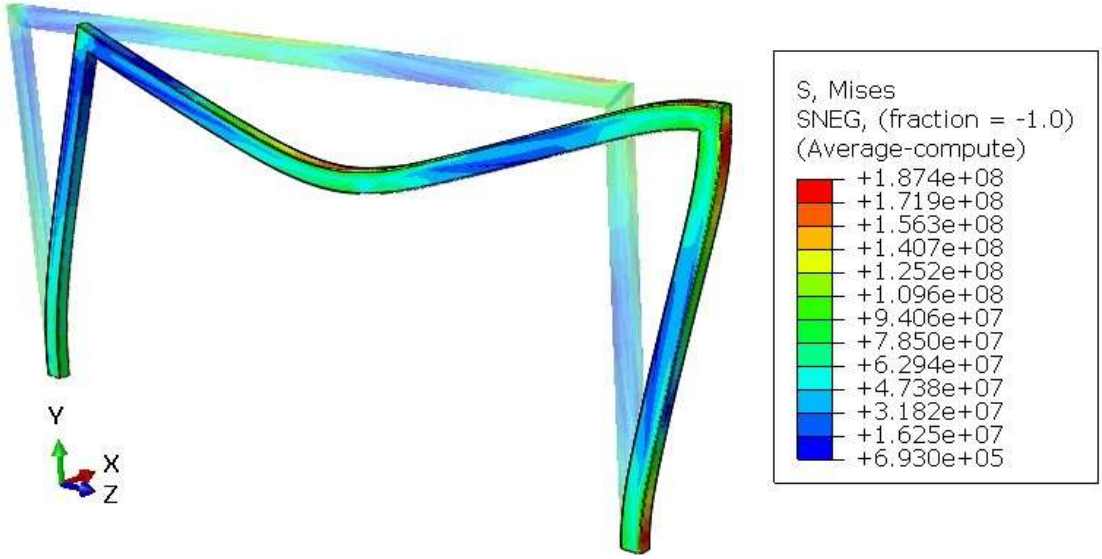

Table 4.11: Von Mises stress distribution (N/m^2) of austenitic (1.4301) stainless steel frame before failure.

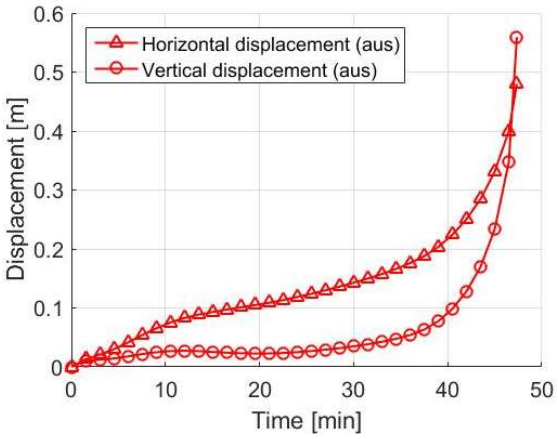

Figure 4.12: Horizontal and vertical displacements over time.

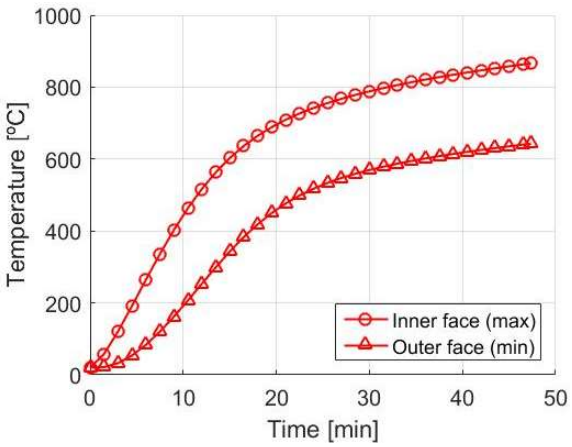

Figure 4.13: Maximum and minimum temperature development over time at every cross-section.

Figure 4.12 shows the increase of the vertical (at midspan) and horizontal displacements as the austenitic stainless steel mechanical properties are being reduced due to fire. When reaching the critical temperature and the time resistance (see Table 4.2), both vertical and horizontal displacement rapidly increase, warning about the frame failure.

The temperature-time relationships of the maximum and minimum temperature of the midspan cross-section for the studied case is presented in Figure 4.13.

The nonuniform temperature distribution within the cross section along the whole frame (see Figure 4.13) induces additional internal forces. This fact may be explained through the analysis of the stress distribution shown in Figure 4.14 corresponding to the mid span section of the beam. At early fire stages tensile and compressive stresses are mainly induced by the bending moment. But as temperature increases and since the beam cannot freely deform the thermal elongation produces high compressive stresses in the upper fibre of the beam. In late fire stages where the displacement restrictions become less effective, this axial compression due to thermal elongation disappears. Previous analytical calculations provided enough knowledge to determine that the last plastic hinge should appear close to the support of the left column. In Figure 4.15 the longitudinal stresses of this critical cross section are presented along with the evolution of $f_{0.2p,\theta}$ and $f_{u,\theta}$ with temperature. It can be seen that failure happens when the longitudinal stress in this section reaches the $f_{u,\theta}$ value, which is dependent on the temperature.

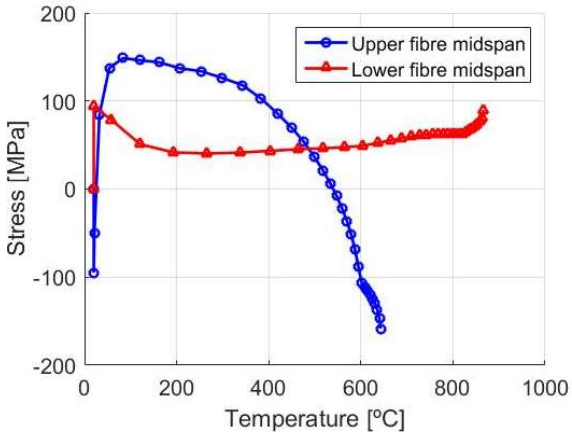

Figure 4.14: Longitudinal stresses versus temperature. Cross section at mid span of the beam.

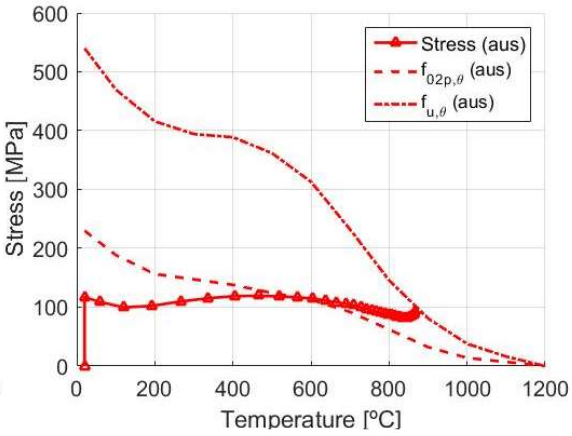

Figure 4.15: Stresses, $f_{0.2p,\theta}$ and $f_{u,\theta}$ values versus temperature. Cross section at the support of the left column.

Normative application

When assessing the design of a structure under fire conditions, the simplified formulation included in the EN 1993-1-2 [21] may be used to determine the critical temperature and, consequently, the time resistance. The simplified formulation is defined in terms of element resistance, consequently it should be applied on the most loaded element, for instance, the right column.

Since there is no specific formulation for stainless steel under fire it should be applied the carbon steel formulation should be applied as it has been explained in Section 2.4. The following expression depends only on the degree of utilization.

$$\theta_{cr} = 39.19 \cdot ln\left(\frac{1}{0.9674 \cdot \mu_0^{3.833}} - 1\right) + 482 \tag{4.11}$$

The degree of utilization μ_0 is referenced to the structural element analysed, since the critical temperature is determined by the critical element of the structure. It can be assumed that the degree of utilization μ_0 of the critical element is the same as the frame degree of utilization of the frame $\mu_0 = 0.3$.

$$\theta_{cr} = 39.19 \cdot ln\left(\frac{1}{0.9674 \cdot 0.3^{3.833}} - 1\right) + 482 = 663.78 \approx 664℃ \tag{4.12}$$

In this studied case, the frame and the elements that form it are susceptible to instability, thus the critical temperature must be iterated until the instability conditions for each element are fulfilled. According to a linear elastic analysis the load applied on the right column are $N_{Ed} = 5.99$ kN, $M_{Ed} = -8.596$ kNm and $\psi M_{Ed} = 8.075$ kNm.

Therefore $N_{b,fi,\theta,Rd}$ can be obtained according to EN 1993-1-2 [21], assuming all partial safety factors as 1:

$$\alpha = 0.65 \cdot \sqrt{\frac{235}{f_y} \cdot \frac{E}{210000}} = 0.64 \tag{4.13}$$

$$\bar{\lambda}_\theta = \frac{k_{y,\theta}}{k_{E,\theta}} \sqrt{\frac{A \cdot f_y}{N_{cr}}} = 0.267 \tag{4.14}$$

$$\phi_\theta = 0.5\left(1 + \alpha\bar{\lambda}_\theta + \bar{\lambda}_\theta^2\right) = 0.621 \tag{4.15}$$

$$\chi_{fi} = \frac{1}{\phi_\theta + \sqrt{\phi_\theta^2 - \bar{\lambda}_\theta^2}} = 0.846 \tag{4.16}$$

$$N_{b,fi,\theta,Rd} = \chi_{fi} k_{y,\theta} A f_y \left(\frac{\gamma_{M0}}{\gamma_{Mfi}}\right) = 183.6\ kN \tag{4.17}$$

Since the right column is subjected to combined bending and axial compression, the following expression must be fulfilled

$$\frac{N_{fi,Ed}}{\chi_{fi} \cdot A \cdot k_{y,\theta} \cdot \frac{f_y}{\gamma_{Mfi}}} + \frac{k_y \cdot M_{y,fi,Ed}}{W_{pl} \cdot k_{y,\theta} \cdot \frac{f_y}{\gamma_{Mfi}}} = 1.29 < 1 \tag{4.18}$$

with

$$W_{pl} = 66772\ mm^3 \tag{4.19}$$

$$k_y = 1 - \frac{\mu_y \cdot N_{fi,Ed}}{\chi_{fi} \cdot A \cdot k_{y,\theta} \cdot \frac{f_y}{\gamma_{Mfi}}} = 0.97 \leq 3 \tag{4.20}$$

where $\mu_y = 0.8$ considers the bending moment distribution along the element. As it can be seen, Eq. (4.18) is not fulfilled. Therefore, the critical temperature θ_{cr} is below 664°C. After some iterations, the critical temperature is $\theta_{cr} = 450$°C can be found.

$$N_{b,fi,\theta,Rd} = \chi_{fi} k_{y,\theta} A f_y \left(\frac{\gamma_{M0}}{\gamma_{Mfi}}\right) = 238.8\ kN \tag{4.21}$$

$$M_{fi,\theta,Rd} = 8.75\ kNm \tag{4.22}$$

$$\frac{N_{fi,Ed}}{\chi_{fi} \cdot A \cdot k_{y,\theta} \cdot \frac{f_y}{\gamma_{Mfi}}} + \frac{k_y \cdot M_{y,fi,Ed}}{W_{pl} \cdot k_{y,\theta} \cdot \frac{f_y}{\gamma_{Mfi}}} = 0.98 \leq 1 \tag{4.23}$$

That means that applying the simplified formulation for temperature development of unprotected steel structures presented in EN 1993-1-2 [21] (see Section 2.4) the time resistance can be calculated.

$$\Delta\theta_{s,t} = k_{sh} \frac{A_m/V}{c_s \rho_s} \dot{h}_{net} \Delta t \tag{4.24}$$

By means of Eq. (4.24) and using the specific stainless steel material properties the computed time resistance is $t_{crit} = 10.9\ min$, far away from the result obtained with more advanced methods $t_{crit} = 40.7\ min$.

This large difference between the results obtained by both methods proves how current codes for design of steel structures under fire situation do not exploit all the advantages that stainless steel structures have in front of fire compared to carbon steel structures. Furthermore, having one face exposed to the outside air contributes to release heat, decreasing the temperature of the steel structure, which is not considered in the formulation included in EN 1993-1-2 [21].

4.3 MATERIAL COMPARISON: STAINLESS STEEL VS. CARBON STEEL

There are 5 basic groups of stainless steel (see Section 2.1), of which austenitic, ferritic and duplex stainless steel are mainly used in building construction. Therefore, the presented results of the austenitic frame under fire are compared with the results of a ferritic stainless steel (1.4003) frame under the same fire conditions, looking for similarities and differences between stainless steel groups. Additionally, both frames response, are compared against a carbon steel (S275) frame under fire, in order to identify potential benefits of stainless steel frames under fire.

The stress-strain relationships at elevated temperatures of the three materials considered in this comparative analysis has been defined according to EN 1993-1-2 [21].

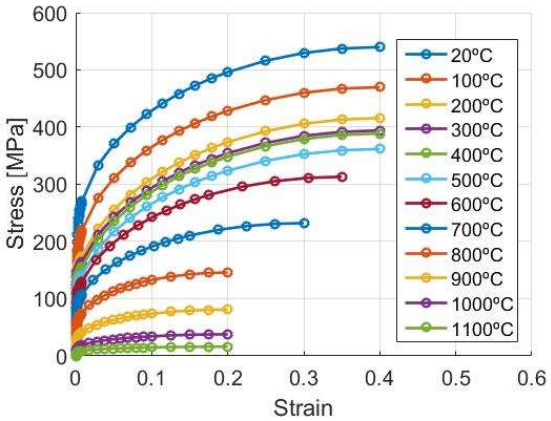

Figure 4.16: Stress-strain relationship at elevated temperatures of austenitic (1.4301) stainless steel.

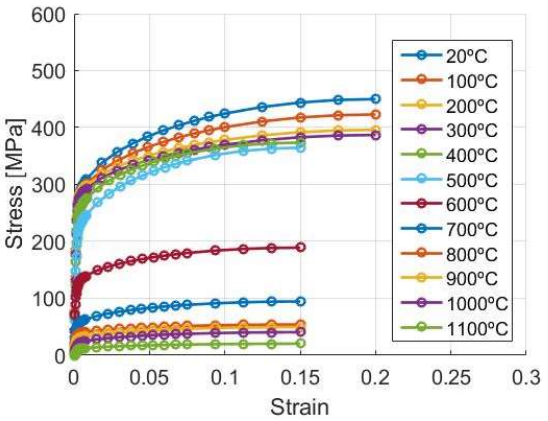

Figure 4.17: Stress-strain relationship at elevated temperatures of ferritic (1.4003) stainless steel.

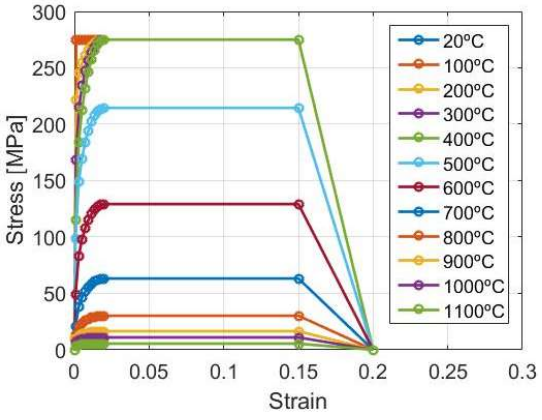

Figure 4.18: Stress-strain relationship at elevated temperatures of carbon (S275) steel.

As it has been already commented, the stainless steel response at elevated temperatures is known to be better. This can be seen in the reduction factors provided in EN 1993-1-2 [21], and shown in Table 4.3, Table 4.4 and Table 4.5.

Temperature	k_E	$k_{f_{0,2}}$	k_{f_u}
20℃	1	1	1
100℃	0.96	0.82	0.87
200℃	0.92	0.68	0.77
300℃	0.88	0.64	0.73
400℃	0.84	0.6	0.72
500℃	0.8	0.54	0.67
600℃	0.76	0.49	0.58
700℃	0.71	0.4	0.43
800℃	0.63	0.27	0.27
900℃	0.45	0.14	0.15
1000℃	0.2	0.06	0.07
1100℃	0.1	0.03	0.03
1200℃	0	0	0

Table 4.3: Austenitic (1.4301) stainless steel reduction factors.

Temperature	k_E	$k_{f_{0,2}}$	k_{f_u}
20℃	1	1	1
100℃	0.96	1	0.94
200℃	0.92	1	0.88
300℃	0.88	0.98	0.86
400℃	0.84	0.91	0.83
500℃	0.8	0.8	0.81
600℃	0.76	0.45	0.42
700℃	0.71	0.19	0.21
800℃	0.63	0.13	0.12
900℃	0.45	0.1	0.11
1000℃	0.2	0.07	0.09
1100℃	0.1	0.035	0.045
1200℃	0	0	0

Table 4.4: Ferritic (1.4003) stainless steel reduction factors.

Temperature	k_E	k_{fp}	k_{fy}
20℃	1	1	1
100℃	1	1	1
200℃	0.9	0.807	1
300℃	0.8	0.613	1
400℃	0.7	0.42	1
500℃	0.6	0.36	0.78
600℃	0.31	0.18	0.47
700℃	0.13	0.075	0.23
800℃	0.09	0.05	0.11
900℃	0.0675	0.0345	0.06
1000℃	0.045	0.025	0.04
1100℃	0.0225	0.0125	0.02
1200℃	0	0	0

Table 4.3: Carbon (S275) steel reduction factors.

Frame response under fire situation

In order to assess and compare the response of steel frames under fire conditions, the same frame geometry with fixed-fixed supports under a design load corresponding to a degree of utilization of $\mu_0 = 0.3$ has been analysed with austenitic, ferritic and carbon steel. The ultimate load at room temperature $R_{fi,d,0}$ of each studied case has been obtained by means of a FE model and it is assumed as the peak load of the load-displacement curve.

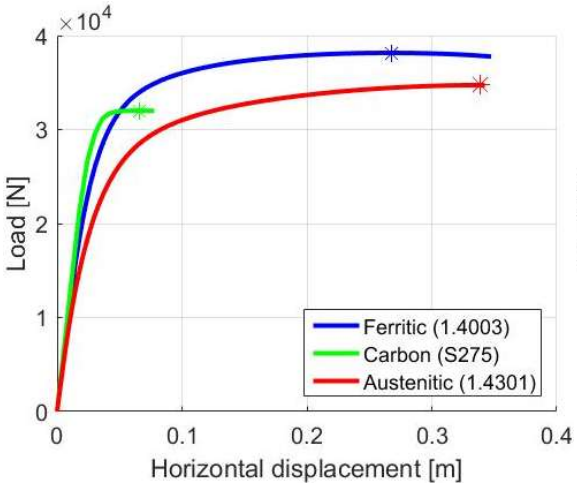

Figure 4.19: Load vs vertical displacement curve at room temperature with different materials.

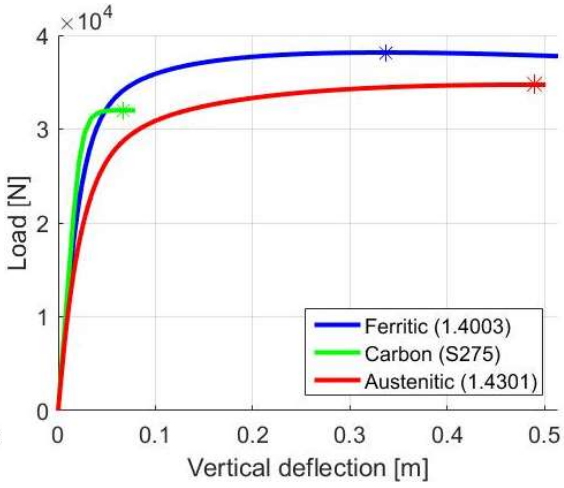

Figure 4.20: Load vs horizontal displacement curve at room temperature with different materials.

As it can be seen, at room temperature, stainless steel frames exhibit larger deflections compared to the carbon steel frame, due to its higher ductility. Figure 4.21 shows the Von Misses stress distribution and the deformed shape of the S275 carbon steel frame.

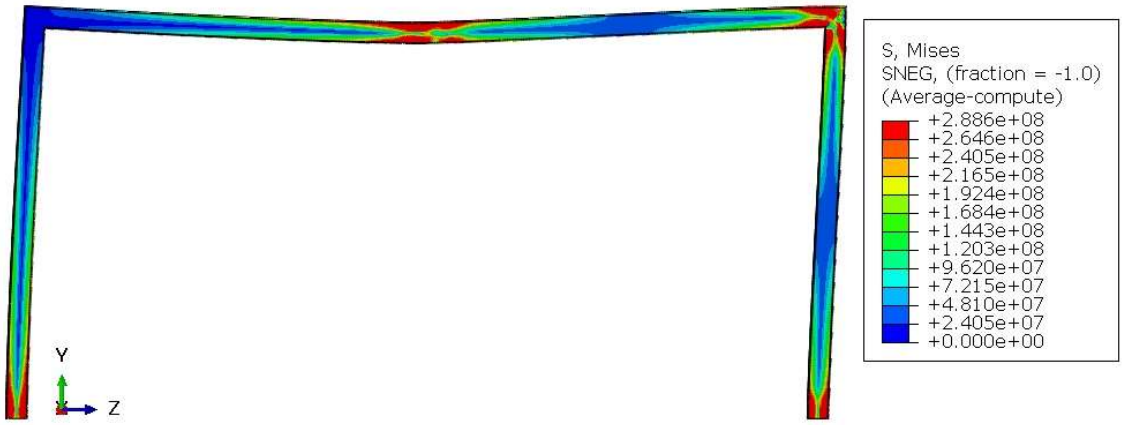

Figure 4.21: Von Misses stress (N/m^2) distribution of the carbon (S275) frame under ultimate load.

Consequently, the thermo-mechanical coupled analysis of each frame has been carried out in the same way that before. Defining an initial load step at room temperature, where the initial load is applied. Afterwards the thermo-mechanical coupled step is carried out where the three inner faces of each section are heated up according to the ISO 834 curve, leaving the outer face in contact with the outside air, permanently at 20℃, and cavity radiation is considered. Time resistance and critical temperatures for all studied cases are shown in Table 4.6.

	Austenitic 1.4301	Ferritic 1.4003	Carbon S275
$R_{fi,d,0}$	34.731 kN	38.156 kN	32.015 kN
Time resistance	47.3 min	23.7 min	23.2 min
Inner face mean temperature	866℃	739℃	715℃
Outer face mean temperature	675℃	545℃	535℃

Table 4.4: Main results of the material comparison obtained from the FE model.

Figure 4.22 shows the vertical and horizontal deflections of the studied cases, increasing both vertical and horizontal deflections as temperature increase and mechanical properties are reduced. In terms of thermal response, the temperature-time relationships for all studied cases (austenitic, ferritic and carbon) are presented in Figure 4.23. Both stainless steel curves are identical because of the thermal properties stated in EN 1993-1-2 [21], are the same for austenitic and ferritic stainless steel, whereas the carbon steel are different because of the thermal properties are not the same. The nonuniform temperature distribution within the cross section along the whole frame induces additional internal forces.

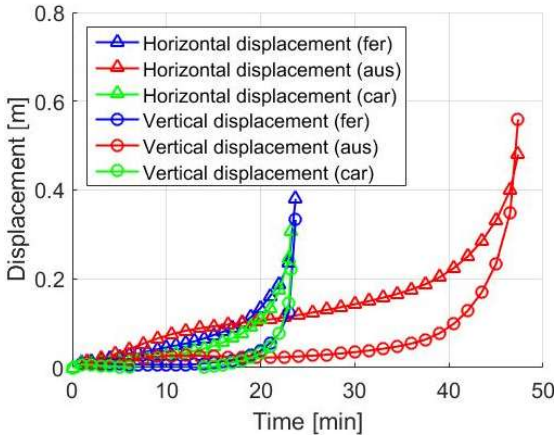

Figure 4.22: Horizontal and vertical displacements over time for austenitic, ferritic and carbon frames.

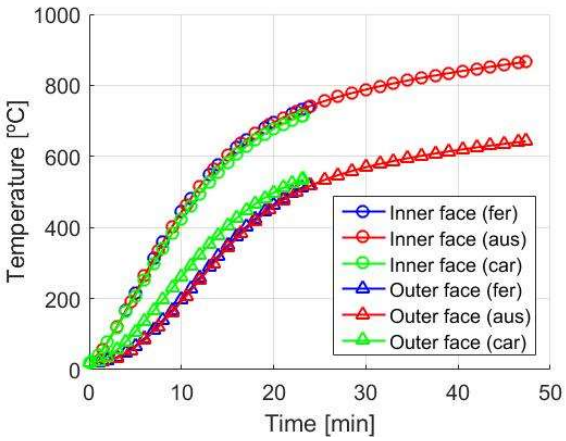

Figure 4.23: Maximum and minimum temperature development over time at every cross-section (for austenitic, ferritic and carbon frames).

All studied cases collapse describing the global plastic mechanism with extensive plastic regions on both supports, on the right joint and on the midspan of the beam (see Figure 4.24).

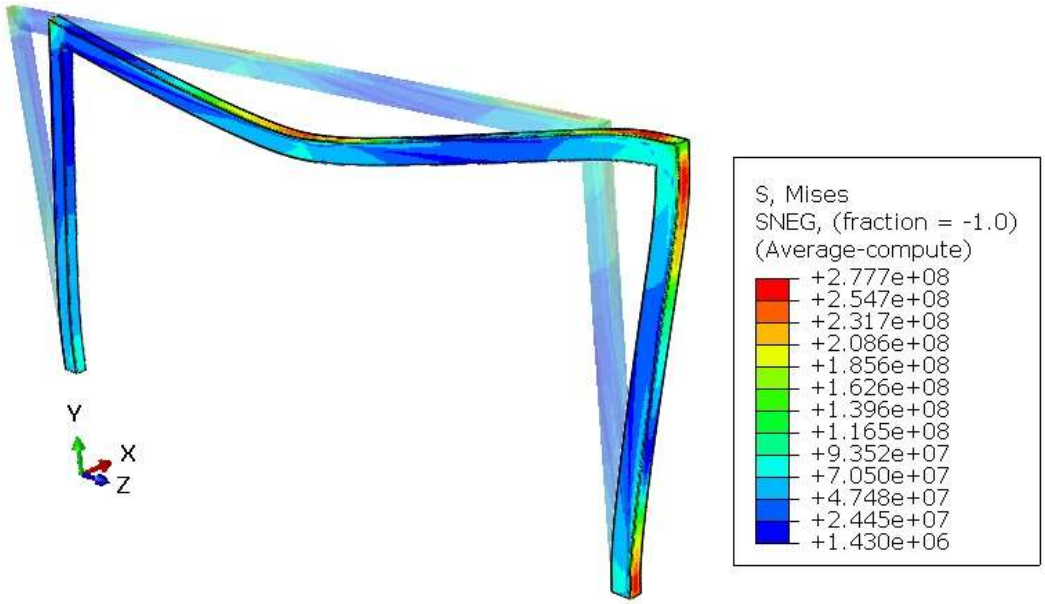

Figure 4.24: Von Misses stress distribution (N/m^2) before collapsing of the ferritic stainless steel frame.

Moreover, previous analytical calculations provided enough knowledge to determine that the last plastic hinge should appear close to the support of the left column. In Figure 4.25 the longitudinal stress of the left support cross section has been plotted along with the evolution of the ultimate stress ($f_{y,\theta}$ or $f_{u,\theta}$) of each material with temperature. It can be seen that in all studied cases the frame collapse when this critical region reaches the ultimate stress, which is dependent on temperature. It should be emphasised how austenitic stainless steel exhibits higher ultimate stress for temperatures above $600℃$, making it able to resist higher temperatures than the other studied cases.

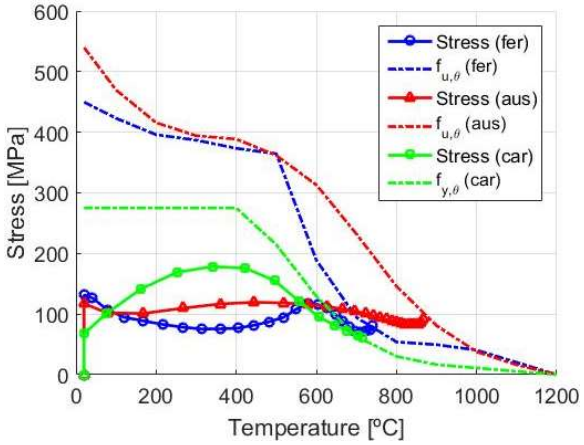

Figure 4.25: Stresses, $f_{y,\theta}$ and $f_{u,\theta}$ values versus temperature. For the cross-section at the support of the left column.

4.4 INFLUENCE OF BOUNDARY CONDITIONS

Boundary conditions are always an important aspect related to the design of a structure, for this reason, in order to achieve an optimal design it is essential to assess the effect of boundary conditions on the response of a structure under fire.

This case of study wants to determine the influence of the mechanical boundary conditions on the response of a steel frame under fire. Due to this fact, the structural response against fire of the austenitic (1.4301) stainless steel frame with fixed-fixed supports is compared with the response of the same stainless steel frame with pinned-pinned supports.

Previous calculations

The pinned-pinned frame under the defined design loads (see Figure 4.26) may show a different response than the already studied fixed-fixed frames. For this reason, the response of the pinned-pinned frame should be previously studied. Since the cross-section defined is Class 1, it can form plastic hinges with the rotation capacity required to form a plastic mechanism.

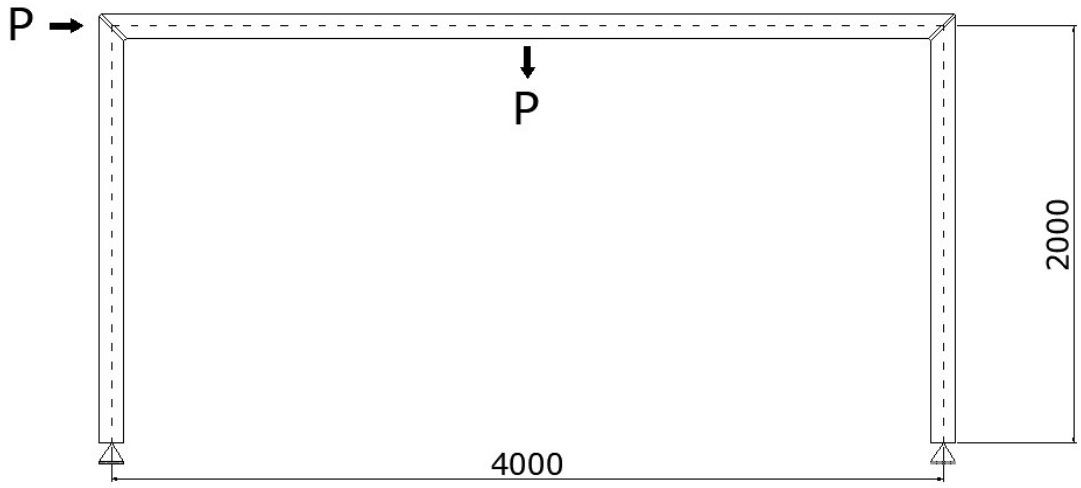

Figure 4.26: Frame geometry (mm) and loads applied of the frame with pinned supports.

The designed frame under the load applied can describe the following plastic failure mechanisms.

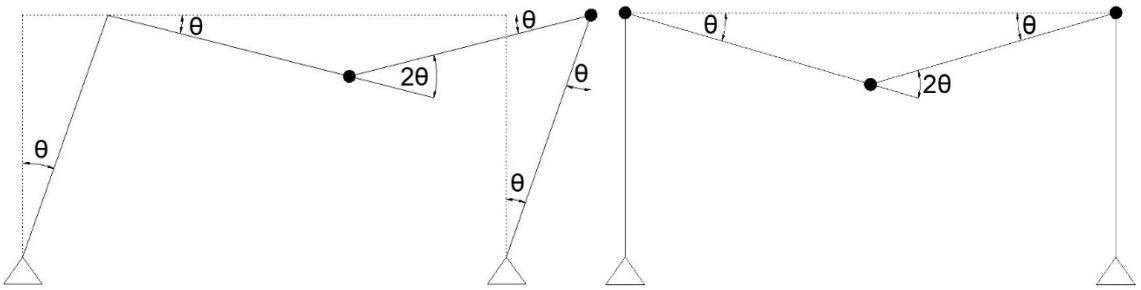

a) Global failure mechanism.

b) Beam failure mechanism.

c) Sway failure mechanism.

Figure 4.27: Possible failure mechanism of a pinned-pinned frame under the loads applied.

As it has been previously done, it can be determined which of the presented failure mechanisms may be the actual response of the frame by the principle of virtual work. The load needed to develop the global failure mechanism of the Figure 4.27.a is the following:

$$W_{int} = 2M_{pl}\theta + 2M_{pl}\theta = 4M_{pl}\theta \tag{4.25}$$

$$W_{ext} = P\delta_H + P\delta_V = 2Pl\theta \tag{4.26}$$

$$P = \frac{2M_{pl}}{l} \tag{4.27}$$

In the same way, the load needed to develop the beam failure mechanism described in Figure 4.27.b can be obtained as:

$$W_{int} = M_{pl}\theta + M_{pl}\theta + 2M_{pl}\theta = 4M_{pl}\theta \tag{4.28}$$

$$W_{ext} = P\delta_V = Pl\theta \tag{4.29}$$

$$P = \frac{4M_{pl}}{l} \tag{4.30}$$

Finally, the load needed to develop the sway failure mechanism described in Figure 4.27.c can be obtained as before.

$$W_{int} = M_{pl}\theta + M_{pl}\theta = 2M_{pl}\theta \tag{4.31}$$

$$W_{ext} = P\delta_H = Pl\theta \tag{4.32}$$

$$P = \frac{2M_{pl}}{l} \tag{4.33}$$

In this case, for the same load value both global and sway failure mechanism could appear. So, by means of a plastic analysis it cannot be determined which of the two possible failure mechanism will develop under the loads applied.

Frame response under fire situation

In the same way that before, in order to assess the influence of the boundary conditions on the response of steel frames under fire conditions, a design load corresponding to a degree of utilization of $\mu_0 = 0.3$ has been applied for both studied cases.

	Fixed-fixed	Pinned-pinned
$R_{fi,d,0}$	34.731 kN	19.068 kN
Time resistance	47.3 min	44.2 min
Inner face mean temperature	866℃	845℃
Outer face mean temperature	675℃	646℃

Table 4.5: Main results of the boundary conditions analysis obtained from the FE model.

The ultimate load at room temperature has been obtained by means of the FE model. For the pinned-pinned frame, the load at which the curvature of the load-displacement curve is null will be assumed as the ultimate load, whereas for the fixed-fixed frame the peak of the load-displacement curve is the ultimate load.

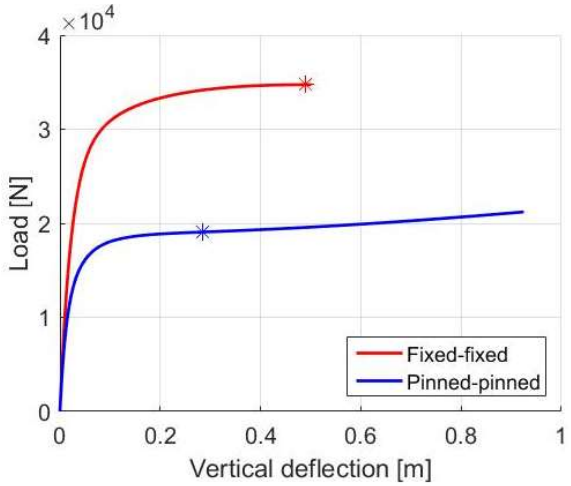

Figure 4.28: Load vs vertical displacement curve for the fixed-fixed and pinned-pinned austenitic frame.

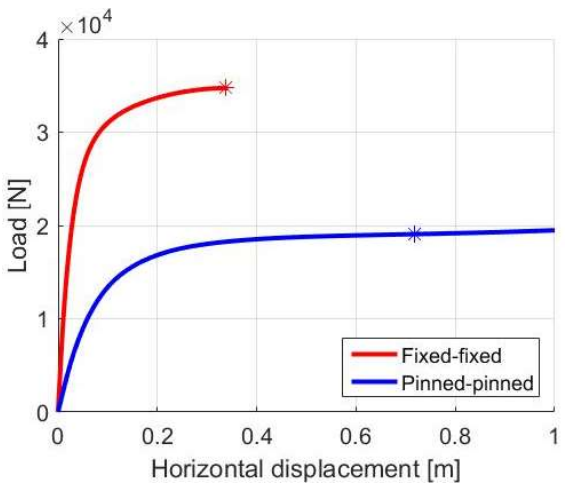

Figure 4.29: Load vs horizontal displacement curve for the fixed-fixed and pinned-pinned austenitic frame.

Figure 4.28 and Figure 4.29 show how the pinned-pinned and fixed-fixed frame response at room temperature. As it was expected the ultimate load for the pinned-pinned frame is lower as previous calculations anticipated. As it can be seen, the fixed-fixed curve shows the typical response of nonlinear material and geometric analysis of the presented frame. On the other hand, the pinned-pinned frame seems to follow this same pattern, but just before the expected failure of the frame, it becomes more rigid, being able to withstand more load. For this reason, it has been decided to assume as the ultimate load at room temperature the load at which the pinned-pinned frame response starts to get stiffer.

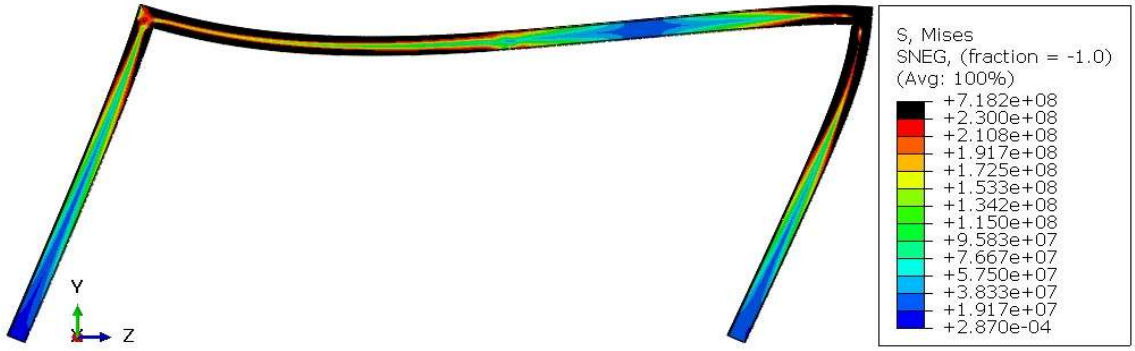

Figure 4.30: Von Mises stress (N/m^2) distribution under the ultimate load at room temperature for the pinned-pinned frame (black regions are elements with stresses over the proof stress $f_{0.2}$).

The pinned-pinned frame seems to developed the sway failure mechanism, but due to material strain hardening the response of the frame becomes stiffer and is able to resist further loads (see Figure 4.30). Then, the thermo-mechanical coupled analysis is carried out, where 3 faces of each section are subjected to fire and the outer face is in contact to the air (permanently at $20℃$). Figure 4.31 shows the temperature distribution for the entire frame, just before collapse.

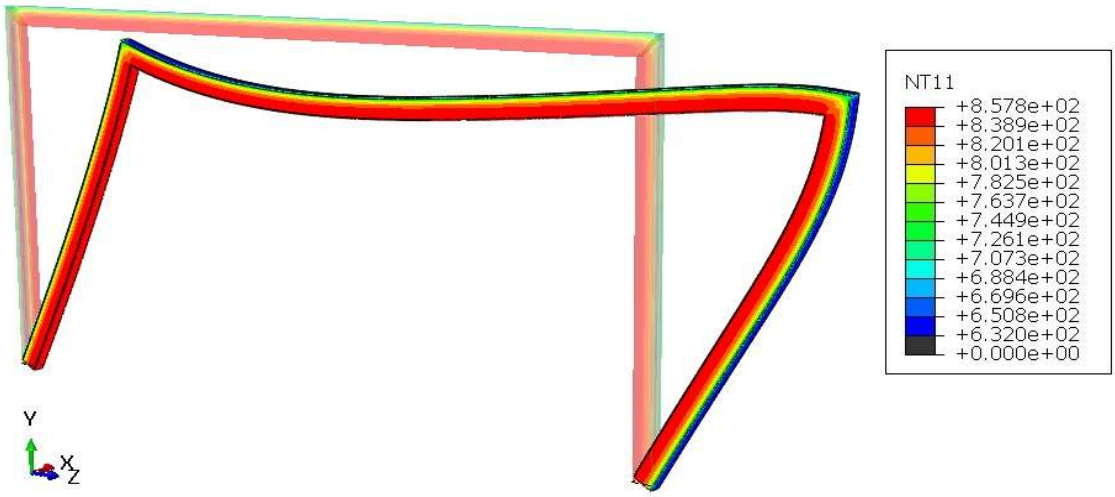

Figure 4.31: Temperature distribution (℃) of the pinned-pinned austenitic (1.4301) frame before collapse.

Figure 4.32 describes the horizontal (HD) and vertical (VD) displacements for both studied cases. The pinned-pinned frame describes larger horizontal displacements at early stages of fire and the time resistance is lower than the fixed-fixed frame. Moreover, the pinned-pinned frame presents lower time resistance than the fixed-fixed frame.

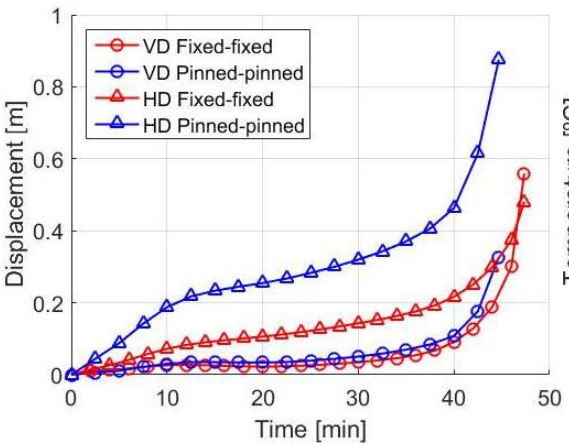

Figure 4.32: Vertical and horizontal displacements over time.

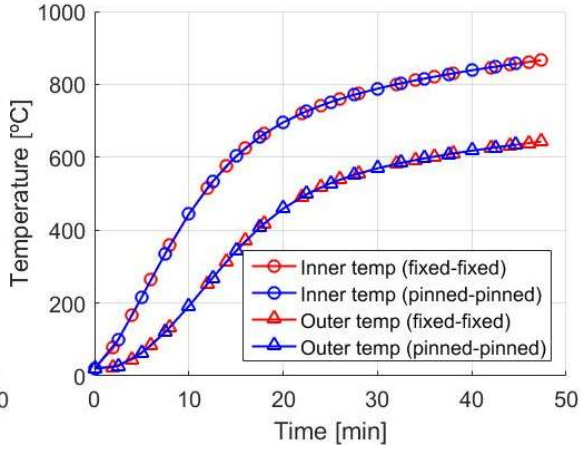

Figure 4.33: Maximum and minimum temperature development over time at every cross-section.

It should be noted that the response of the pinned-pinned frame subjected to fire describes also a sudden increase on the stiffness response. It has been assumed as frame collapse under fire when the curvature of the time-displacement curve is null. The further converged steps after the assumed frame collapse are not presented in Figure 4.32. In terms of temperature development, no difference can be seen between both studied cases (see Figure 4.33) meaning that the mechanical problem seems to not have much effect on the thermal response of the structure under fire.

4.5 INFLUENCE OF THE DEGREE OF UTILIZATION

As it has been already introduced, the combination of actions under fire situation considers lower values of the safety factor for loads ($\gamma_G = 1.0$, $\gamma_Q = 1.0$) than at room temperature ($\gamma_G = 1.35$, $\gamma_Q = 1.5$) (see Section 2.4). For the verification of the Ultimate Limit State at room temperature, the structure should be designed to withstand the ultimate load $R_{fi,d,0}$. Therefore, when assessing the response of the structure under fire only a fraction of such ultimate load at room temperature should be applied. In the worst-case scenario, all loads considered at room temperature would be applying when

the fire starts, but with lower partial safety factors, this means that the maximum degree of utilization can be approximated to:

$$\mu_{0,max} = \frac{R_{fi,d,t}}{R_{fi,d,0}} \approx \frac{(1+1)\cdot P}{(1.35+1.5)\cdot P} = 0.7 \tag{4.34}$$

In order to assess the influence of initial load on the frame resistance under fire, the austenitic stainless steel frame with fixed-fixed supports is subjected to different degrees of utilization (0.2, 0.3, 0.4, 0.5, 0.6, 0.7).

	Initial load	Time resistance	Inner face temperature	Outer face temperature
$0.2 \cdot R_{fi,0}$	6.946 kN	79.6 min	945°C	713°C
$0.3 \cdot R_{fi,0}$	10.419 kN	47.3 min	866°C	675°C
$0.4 \cdot R_{fi,0}$	13.892 kN	30.3 min	791°C	572°C
$0.5 \cdot R_{fi,0}$	17.365 kN	20.2 min	698°C	463°C
$0.6 \cdot R_{fi,0}$	20.839 kN	12.6 min	537°C	272°C
$0.7 \cdot R_{fi,0}$	24.311 kN	6.8 min	302°C	102°C

Table 4.6: Main results of the degree of utilization analysis obtained from the FE model.

Table 4.8 shows how frames with lower degree of utilization present higher time resistances. Frames with higher degree of utilization exhibit larger initial vertical (VD) and horizontal (HD) deflections (see Figure 4.34), making them more sensitive to second order geometric effects that are amplified by the reduction of mechanical properties at elevated temperatures.

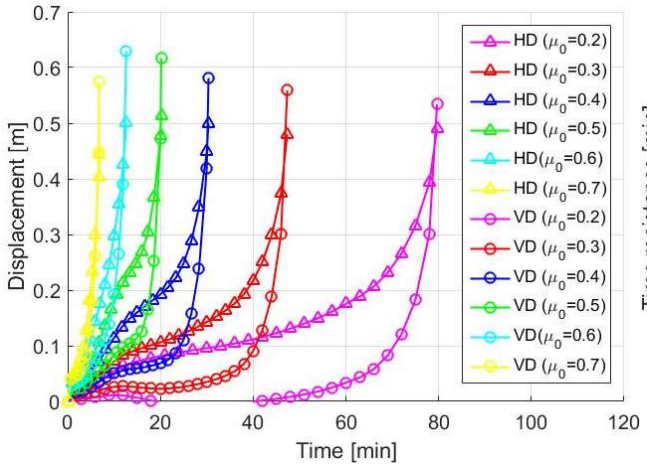

Figure 4.34: Vertical and horizontal displacements over time depending on degree of utilization.

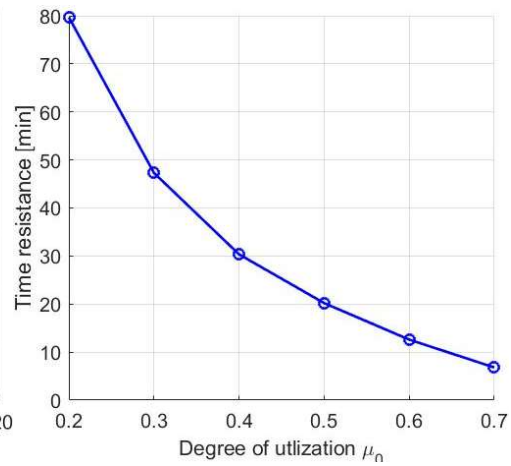

Figure 4.35: Time resistance depending on the degree of utilization.

Figure 4.35 shows the time resistance for different degrees of utilization. As expected, higher degree of utilization leads to lower time resistance. Furthermore, the time

resistance does not increase linearly with the degree of utilization. For instance, going from a degree of utilization of $\mu_0 = 0.7$ to $\mu_0 = 0.6$ increases the time resistance in 5.8 min, whereas reducing it from $\mu_0 = 0.3$ to $\mu_0 = 0.2$ increases the time resistance in 32.4 min.

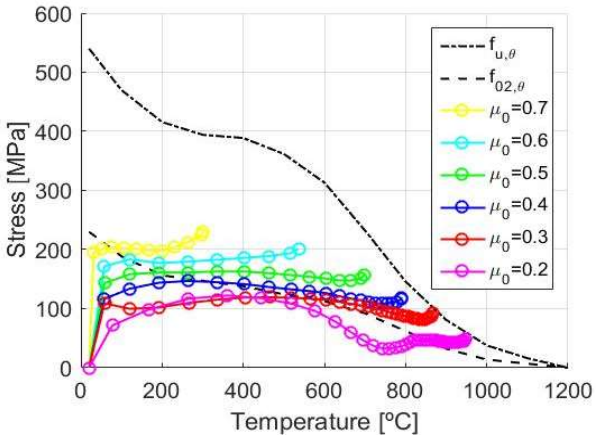

Figure 4.36: Longitudinal stress development over time of the left support section for different degrees of utilization.

The frame shown in Section 4.1 (austenitic stainless steel frame with fixed supports) collapsed when the last plastic hinge formed in the left support and described the global failure mechanism. However, Figure 4.36 shows very clearly the influence of the initial load applied on the type of failure of the austenitic steel frame. Then, the frame collapses before forming a plastic hinge in the left support, meaning that in those studied cases with a degree of utilization $\mu_0 \geq 0.4$, the frame does not describe the global failure mechanism but fails due to global frame instability. From the results obtained, it can be inferred that for higher initial loads (higher degree of utilization) the frame collapses for a stress distribution on the left support far from the ultimate stress $f_{u,\theta}$, meaning that the second order geometric effects have a higher impact on the structure response for higher degrees of utilization, preventing the development of the global failure mechanism.

CHAPTER 5

5. CONCLUSIONS AND FUTURE WORKS

5.1 SUMMARY

In the present document the current knowledge about the structural response of stainless steel structures subjected to fire and how it is implemented in the current European codes has been discussed (see Chapter 2). Furthermore, Chapter 3 explains the advanced numerical model developed to accurately reproduce the thermal and mechanical problems of stainless steel structures subject to fire. Additionally, a simplified model has been developed to reproduce the effect of cavity radiation on the heat transfer problem of hollow sections with satisfactory results.

Chapter 4 presents the thermal and structural analysis of stainless steel frames subjected to fire by means of thermo-mechanical coupled analysis. In this chapter, a parametric study has been carried out in order to identify key aspects of the structural response of carbon and stainless steel frames subject to fire and assess the influence of the most relevant variables governing the problem. The main conclusions of this document are presented below.

5.2 NUMERICAL MODEL

The main goal when calibrating the numerical model was proving that it was able to reproduce the real response of steel structures subjected to fire. For this reason, the numerical model has been validated against multiple numerical and experimental results from the literature with satisfactory results.

Thanks to the thorough analysis of the numerical model there are four main points that should be remarked about the numerical model:

- When assessing the thermal response of steel structures under fire there are thermal material parameters involved in the thermal response, such as material emissivity or the convection coefficient that have been determined by previous researchers by means of numerical and experimental tests. Carbon steel thermal parameters have been deeply studied, whereas the stainless steel thermal properties are still a topic of discussion between researchers. For all the developed models in this research, the values used for stainless steel emissivity and the convective coefficient are $\varepsilon = 0.4$ and $\alpha_c = 25\mathrm{W/m^{2}{}^{\circ}K}$ respectively, because it reproduced more accurately the temperature development.
- From the literature such values could be found how in many cases when assessing the thermal response of a hollow section element the cavity heat transfer has not been considered in the numerical model. With the objective of assessing the influence of the cavity radiation in the overall response of the structure, a simplified numerical method has been developed to assess the gas temperature inside the cavity of a hollow section. Furthermore, it has been validated against the simplified method for cavity radiation included in Abaqus with satisfactory results. It has been proved that including the cavity heat transfer in the thermo-mechanical coupled analysis of a structural element subjected to fire in three of its four faces, not only affects the thermal response, but increase the time resistance of the structural element.
- One of the main goals of this dissertation was to prove the necessity to assess the response of a structure under fire by means of anisothermal tests, not by means of multiple numerical and experimental isothermal tests, because real

structures are already loaded when fire starts and then the temperature of the structure increases until is not able to resist anymore the initial loads applied. Moreover, the response of the whole structure under fire should not be tied to the structural element in worst conditions, because steel structures are able to redistribute the loads applied when one element or section reaches the yield stress, even more for stainless steel structures, where strain hardening plays a beneficial role in the post yielding behaviour and this should be considered in the structural design under fire conditions.

- When assessing the response of structures under fire, carrying out a thermo-mechanical coupled analysis is the optimal way to go, but it greatly increases the computational cost of the problem. In the studied cases, namely, structures with uniform cross-section along the element and equal fire conditions for each cross-section, it has been proved that large displacements of the structure do not affect the thermal response of it and consequently this type of problems can be addressed with a sequentially thermo-mechanical analysis.

5.3 STAINLESS STEEL FRAMES

The main objective of this document was to assess the response of stainless steel frames under fire and it can be said that this objective has been fulfilled. A parametric study has been carried out, aiming to identify key aspects that rule the structural response of stainless steel frames under fire. Thanks to this study, there are some topics that should be pointed out:

- The current version of EN 1993-1-2 [21] does not provide a suitable formulation for stainless steel structures subjected to fire as it has been proved, meaning that the design of stainless steel structures subjected under fire situation is far from being optimal.
- From the analysis of the material influence on the structural response of the frame subjected to fire, it can be pointed out that austenitic stainless steel frames show a better response under fire than carbon steel frames, presenting larger time resistance and higher critical temperature. At the same time, ferritic stainless steel frames seems to present no benefit in terms of fire resistance

compared to carbon steel frames, but exhibit larger displacements before the frame collapse due to their higher ductility. Nonetheless, with a detailed structural analysis, austenitic stainless steel structures may not need passive fire protection to fulfil the design requirements for evacuation, reducing the material and execution cost of the building project and contributing to a more economical design of stainless steel structures compared to carbon steel structures.

- Boundary conditions have a direct effect on the frame response under fire scenarios. Larger initial displacements of the pinned-pinned frame make it more sensitive to second order geometric effects, leaving it in worse conditions to cope with fire. When fire starts, the structure temperature increases and as a result the steel mechanical properties get reduced, boosting the initial displacements and aggravating the second order geometric effects of the structure.
- Lastly, it can be concluded that the initial loads applied on the structure before the fire starts directly influence the fire resistance of the frame. Not only that, but they also determine the way the frame collapses. For higher values of the degree of utilization the frames collapsed due to second order effects, far from their ultimate strength, whereas for lower values of the degree of utilization, the frames described the collapse failure mechanism previously calculated Therefore, determining the combination of loads applied under fire situation is essential to correctly assess the structural response of stainless steel frames under fire.

5.4 FUTURE WORKS

The main objective in the future should be to continue with the parametric study of stainless steel frames, assessing the influence of other potential key aspects on the structure response and compare the results obtained with the next update of EN 1993-1-2 [21] and EN 1993-1-4 [17]. Some directions of further research could be:

- As it has been explained, the stress-strain relationship of the stainless steel at elevated temperatures is still a topic of discussions nowadays. The current stress-strain relationship included in EN 1993-1-2 [21] seems to be too much in the safe

side, which is why there are other publications such as the *Design Manual for Structural Stainless Steel* [6] that include an alternative formulation for the stress-strain relationship of stainless steel at elevated temperatures with different values for the reduction factors. For this reason, a good way to go for further research would be to determine the properties of different grades of stainless steel by means of experimental tests, including thermal properties, stress-strain relationships and reduction factors.

- Another direction of research would be to assess the influence of different types of section on the structural response in front of fire. L-shape or I-shape sections do not receive the same amount of heat on all its faces when exposed to fire, resulting in a different thermal and mechanical response of the structure. Studying different types of section would help to determine which type of sections have a better response in front of fire.
- In the present work only Class 1 sections have been analysed under fire conditions. Another field of study would be to assess the influence of the section class on the response of a steel structure under fire. But, more specifically, the response of Class 4 sections under fire, because right now the EN 1993-1-2 [21] states that the critical temperature for Class 4 sections is $350℃$. This limit was set based on studies carried on carbon steel elements, but since austenitic stainless steel seems to resist better the fire action, this limitation may not be appropriate for stainless steel structures.
- Additionally, in this research only frames with the same section along it have been analysed. The influence of a nonuniform section in the response under fire may be really interesting, because not only influences directly to the structural response, but also a nonuniform section would mean a longitudinal heat flux along the structure that in the present study has not been considered.
- An interesting direction of research would be assessing the response of stainless steel frames protected against fire with passive protection. Because assessing the influence of passive protection on the fire resistance of a stainless steel structure may be determining for an optimal structural design under fire conditions. Additionally, other types of conditions, such as concrete coating or

localised fires, could be included in further studies in order to assess if it is beneficial or not on the structure response under fire.

- Finally, all the studies carried out and further studies to come should be used to establish specific formulation for stainless steel structures subjected to fire.

BIBLIOGRAPHY

[1] Baddoo N. R. 100 years of stainless steel: A review of structural applications and the development of design rules. The Structural Engineer, 91:10-8, 2013.

[2] Gardner, L. & Cruise, R. B. & Sok, C. P. & Krishnan, K. & Ministro Dos Santos, J. Life-cycle costing of metallic structures. Proceedings of the Institution of Civil Engineers. Engineering Sustainability, 160(4):167-177, 2007.

[3] Rossi, B. Discussion on the use of stainless steel in constructions in view of sustainability. Thin-Walled Structures, 83:182-189, 2013.

[4] Gardner, L. Stainless steel structures in fire. Proceedings of the Institution of Civil Engineers - Structures and Buildings. 160(3), 129-138, 2007.

[5] UNE-EN 10088-1:2015: Stainless steels - Part 1: List of stainless steels.

[6] Design Manual of Structural Stainless Steel. 4th Edition. Ascot, United Kingdom, 2007. ISBN: 978-1-85942-226-7.

[7] ESDEP, Programa Europeo de Formación en el Cálculo y Diseño de la Construcción en Acero. Instituto Técnico de la Estructura en Acero (ITEA), 2000.

[8] Dundu, M. Evolution of stress-strain models of stainless steel in structural engineering applications. Construction and Building Materials, 165, 413-423, 2018.

[9] Technical Note No. 902. Ramberg, W. & Osgood, W.R. Description of stress-strain curves by three parameters. Washington, D.C., USA: National Advisory Committee for Aeronautics, 1943.

[10] Ashraf, M. & Gardner, L. & Nethercot, D.A. Finite element modelling of structural stainless steel cross-sections, Thin-Walled Structures 44 (10) 1048–1062, 2006.

[11] Ramberg, W. & Osgood, W.R. Description of stress–strain curves by three parameters. Technical Note No. 902, National Advisory Committee for Aeronautics, Washington DC, 1943.

[12] H.N. Hill, Determination of stress–strain relations from the offset yield strength values. Technical Note No. 927, National Advisory Committee for Aeronautics, Washington DC, 1944.

[13] Standards Australia & Standards New Zealand Australian/New Zealand Standard: Cold-formed stainless steel structures. Sydney, Australia, 2001. ISBN: 0-7337-3979.

[14] American Society of Civil Engineers & Structural Engineering Institute Specification for the Design of Cold-Formed Stainless Steel Structural Members. Reston, Virginia, 2002. ISBN 0-7844-0556-5.

[15] Mirambell, E. & Real, E. On the calculation of deflections in structural stainless steel beams: an experimental and numerical investigation. Journal of Constructional Steel Research, 4. 54 (1), 109-133, 2000. ISSN 0143-974X. doi: DOI: 10.1016/S0143-974X(99)00051-6.

[16] Rasmussen, K.J.R. Full-range stress–strain curves for stainless steel alloys. Journal of Constructional Steel Research, 1. 59 (1), 47-61, 2003. ISSN 0143-974X. doi: DOI: 10.1016/S0143-974X(02)00018-4.

[17] EN 1993-1-4: 2006. Eurocode 3: Design of steel structures – Part 1-4: General rules – Supplementary rules for stainless steels. Brussels: European Committee for Standardization

[18] Gardner, L. & Ashraf, M. Structural design for non-linear metallic materials. Engineering Structures, 5. 28(6), 926-934, 2006. ISSN 0141-0296.

[19] Chen, J. & Young, B. Stress–strain curves for stainless steel at elevated temperatures, Engineering Structures. 28, 229–239, 2006.

[20] Gardner, L. & Insausti, A. & Ngb, K.T., Ashraf, M. Elevated temperature material properties of stainless steel alloys, Journal of Construction Steel Research. 66, 634–647,2010.

[21] EN1993-1-2:2005. Eurocode 3: Design of steel structures – Part 1-2: General rules – Structural fire design. Brussels: European Committee for Standardization.

[22] Abdella, K. Inversion of a full-range stress-strain relation for stainlesss steel alloys. International Journal of Non-Linear Mechanics, 41, 456-463, 2006.

[23] EN1993-1-2:20XX, annex C. Eurocode 3: Design of steel structures – Part 1-2: General rules – Structural fire design. Brussels: European Committee for Standardization. (Document under revision)

[24] Lawrence J. Fennelly. Effective Physical Security, 4th Edition. Butterworth-Heinemann, 2013. ISBN: 978-0-12-415892-4.

[25] Alarifi, A. & Phylaktou, R. & Andrews, G. What Kills People in a Fire? Heat or Smoke? The 9th Saudi Students Conference, Birmingham, United Kingdom, 2006.

[26] Ganji, D. & Sabzehmeidani, Y. & Sedighiamiri, A. Nonlinear Heat Transfer: Mathematical Modeling and Analytical Methods. Elsevier Science, 2018. ISBN: 978-0-12-812024-8

[27] Gardner, L. & Ng, K.T. Temperature development in structural stainless steel sections exposed to fire. Fire Safety Journal, 41, 185-203, 2006.

[28] Guide to the advanced fire safety engineering of structures. Ascot, United Kingdom, 2007. ISBN: 978-0-901297-46-4.

[29] Design of Columns Subject to Localised Fires. Ascot, United Kingdom, 2018. ISBN 13: 978-1-85942-240-3.

[30] EN 1991-1-2:1995. Eurocode 1: Actions on structures – Part 1-2: General actions –Actions on structures exposed to fire. Brussels: European Committee for Standardization.

[31] Implementation of Eurocodes. HandBook5: Design of Building for the Fire Situation. Luxemburg, 2005.

[32] EN 1990:2002. Eurocode 0: Basis of structural design. Brussels: European Committee for Standardization.

[33] Código Técnico de la Edificación, Documento Básico, Seguridad ante Incendio. CTE-DB-SI. Ministerio de Fomento, España, 2006.

[34] Fan, S. & Jia, L. & Lyu, X. & Sun, W. & Chen, M. & Zheng, J. Experimental investigation of austenitic stainless steel material at elevated temperatures. Construction and Building Material, 155, 267-285, 2017.

[35] Tondini, N. & Rossi, B. & Franssen, JM. Experimental investigation on ferritic stainless steel columns in fire. Fire Safety Journal, 62, 238-248, 2013.

[36] Fan, S. & He, B & Xia, X. & Gui, H. & Liu, M. Fire resistance of stainless steel beams with rectangular hollow section: Experimental investigation. Fire Safety Journal, 81, 17-31, 2016.

[37] Fan, S. & Zhang, L. & Sun, W. & Ding, X. & Liu, M. Numerical investigation on fire resistance of stainless steel columns with square hollow section under axial compression. Thin-Walled Structures, 98, 185-195, 2016.

[38] Abaqus Documentation. Abaqus 2016. Abaqus, Version 6.16. Dassault Systmes Simulia Corp. USA.

[39] EN 1993-1-1: 2001. Eurocode 3: Design of steel structures – Part 1-1: General structural rules Brussels: European Committee for Standardization.

[40] Hibbeler, R.C. Mechanics of materials 8th edition. Pearson, 1997. ISBN 13: 978-9-81068-509-6.

[41] Gillie, M. Analysis of heated structures: Natures and modelling benchmarks. Fire Safety Journal, 44, 673-680, 2009.

[42] Vila-Real, P. & Lopes, N. & Simoes da Silva, L. & Franssen, JM. Lateral–torsional buckling of stainless steel I-beams in case of fire. Journal of Constructional Steel Research, 64, 1302-1309, 2008.

[43] Ellobody, E. & Feng, R. & Young, B. Finite Element Analysis and Design of Metal Structures. Butterworth-Heinemann, 2014. ISBN: 978-0-12-416561-8.

[44] Walport, F. & Gardner, L. & Real, E. & Arrayago, I. & Nethercot, D.A. Effects of material nonlinearity on the global analysis and stability of stainless steel frames. Journal of Constructional Steel Research, 152, 173-182, 2019.

[45] Rossi, B. Stainless steel in structures in view of sustainability. In: Fourth international stainless steel experts seminar. Ascot, UK, 2012.

[46] Afshan, S. Structural Behaviour of Cold-Formed Stainless Steel Tubular Members. PhD thesis, Imperial College London, 2013.

[47] Çengel, Y. & Cimbala, J. Fuild Mechanics: Fundamental and application, 1st Edition. Mc GrawHill, 2006. ISBN: 970-10-5612-4.

[48] Arrayago, I. & Real, E. & Mirambell, E. Prelminary study and tests arrangements for experimental programme on stainless steel frames. 9th Conference on Steel and Aluminium Structures (ICSAS19). Bradford, United Kingdom, 2019.

[49] Zhan, K. & Wu, X.Y. & Jiang, C.H. & Ji, V. Thermal Relaxation Behaviour of Residual Stress and Microstructure in Shot Peened S30432 Steel at Elevated Temperatures. Materials Transactions, 53(6), 1195-1198, 2010.

Other bibliography that have been used, but is not mentioned in the document:

Carslaw, H.S. & Jaeger, J.C. Conduction of Heat in Solids. Cambridge, United Kingdom: Oxforn University Press, 1959. ISBN: 0-19-853303-9.

SIF'06 Proceedings of the 4th international workshop: structures in fire, 1-2. Universidade de Aveiro, 2006. Edited by: Vila-Real, Paulo & Franssen, J.M & Lopes, N. ISBN: 972-789-190-X

Mirambell, E. Criterios de Diseño en Puentes de Hormigón Frente a la Acción Térmica ambiental. Tesis de Doctorado, UPC, 1987.